4-2020

Comparison of Optimal Energy Management Strategies Using Dynamic Programming, Model Predictive Control, and Constant Velocity Prediction

Amol Arvind Patil
Western Michigan University, amolp.patl188@gmail.com

COMPARISON OF OPTIMAL ENERGY MANAGEMENT STRATEGIES USING DYNAMIC PROGRAMMING, MODEL PREDICTIVE CONTROL, AND CONSTANT VELOCITY PREDICTION

by

Amol Arvind Patil

A thesis submitted to the Graduate College
in partial fulfillment of the requirements
for the degree of Master of Science in Engineering
Mechanical Engineering
Western Michigan University
April 2020

Thesis Committee:

Dr. Zachary Asher, Ph. D., Chair
Dr. Richard Meyer, Ph. D.
Dr. Jennifer Hudson, Ph. D.

COMPARISON OF OPTIMAL ENERGY MANAGEMENT STRATEGIES USING DYNAMIC PROGRAMMING, MODEL PREDICTIVE CONTROL, AND CONSTANT VELOCITY PREDICTION

Amol Arvind Patil, M.S.E.

Western Michigan University, 2020

Due to the recent advancements in autonomous vehicle technology, future vehicle velocity predictions are becoming more robust which allows fuel economy (FE) improvements in hybrid electric vehicles through optimal energy management strategies (EMS). A real-world highway drive cycle (DC) and a controls-oriented 2017 Toyota Prius Prime model are used to study potential FE improvements. We proposed three important metrics for comparison: (1) perfect full drive cycle prediction using dynamic programming, (2) 10-second prediction horizon model predictive control (MPC), and (3) 10-second constant velocity prediction. These different velocity predictions are put into an optimal EMS derivation algorithm to derive optimal engine torque and engine speed. The results show that the constant velocity prediction algorithm outperformed the baseline control strategy but underperformed the MPC strategy with an average 1.58% and 2.45% of FE improvement with highway and city-highway DC. Also, using a 10-second prediction window MPC strategy provided FE improvement results close to the full drive cycle prediction case. MPC has the potential to achieve **60%-65%** and **70% - 80%** of global FE improvement over highway and city-highway DC respectively.

ACKNOWLEDGMENTS

I would like to thank Dr. Zachary Asher of the Mechanical and Aerospace Engineering Department at Western Michigan University for granting me the opportunity to work on this project and for supporting me during every step of my research. I would like to thank Dr. Richard Meyer and Dr. Jennifer Hudson for providing valuable inputs and serving on this thesis committee. This journey would not be so wonderful without the help and support of the great people at the “Energy Efficient & Autonomous Vehicles Laboratory” of Western Michigan University.

This material is based upon work supported by the U.S. Department of Energy's Office of Energy Efficiency and Renewable Energy (EERE). The specific organization overseeing this report is the Vehicle Technologies Office under award number DE-EE0008468.

Amol Arvind Patil

TABLE OF CONTENTS

Table of Contents - Continued

LIST OF TABLES

LIST OF FIGURES

Table of Figures – Continued

Table of Figures – Continued

1. INTRODUCTION

Transportation-related air pollution issues have gained increasing attention in recent years. Federal and state governments have mandated that new transportation projects conform to the Environmental Protection Agency (EPA) regulations. Advancement in novel vehicle control approaches that accomplish improved fuel economy is an ongoing topic of study due to the financial, environmental, and air-pollution impact of transportation [1, 2, 6]. Improving fuel economy (FE) is an important way to reduce the adverse effects of climate change and reduce energy use [2, 3, 6]. This FE improvement along with a significant reduction in emissions has been achieved using hybrid electric vehicles (HEVs) and plug-In hybrid electric vehicles (PHEVs).

Modern-day vehicles are equipped with an ability to comprehend the worldview with many sophisticated sensors and signals and the industry is moving rapidly towards the "Intelligent Vehicle Era" [4, 6]. An intelligent vehicle means a vehicle that can sense the environment around it, communicate with it, and execute the controls accordingly. The type of sensors/signals available is vehicle-to-vehicle (V2V)/ vehicle-to-vehicle (V2I) communication, advanced driver-assistance systems (ADAS - RADAR, LiDAR, Camera), traffic data, controller area network (CAN) data and GPS [5, 7, 8]. Those modern-day technologies can tremendously improve vehicular safety along with reduced energy consumption and reduced environmental pollution [2].

There are two types of vehicle control strategies that can effectively improve the FE (1) driving behavior modification including eco-driving and eco-routing, (2) powertrain operation modification through optimal energy management strategy (EMS) [6, 9]. The optimal EMS can be classified as (1) instantaneous second by second optimization without prior knowledge of whole drive cycle (DC) and (2) predictive optimal EMS which requires some trip information known beforehand [6, 10, 11].

Furthermore, predictive optimal EMS can be classified as- 1) globally optimal EMS with perfect full DC knowledge and prediction by using numerical optimization methods like

dynamic programming (DP) and pontryagin's minimum principle (PMP) [6, 10, 12] (2) non-globally optimal EMS with stochastic prediction and computationally efficient non-global optimal EMS [6, 13, 14]. The last two methods don't guarantee the global solution but come with less computational cost and are practically implementable.

When deriving a globally optimal EMS using deterministic prediction, DP has been the overwhelming favorite due to its ease of use, robustness, and no need for knowledge of derivatives [6, 10,15]. A globally optimal EMS with deterministic prediction is difficult to implement in practice because of the high computational cost and deviations in the planned for drive due to disturbances that arise from interaction with traffic, traffic control devices, etc., but it is still beneficial in simulation to define the upper practical limit on FE benefits for a given vehicle and drive cycle [6, 16]. Computationally efficient non-global optimal EMS can be implemented by model predictive control (MPC), where the optimization is done over a moving finite horizon that is shorter than the DC. Also, with the advancement in perception systems and associated computational improvements, MPC is implementable in real vehicles [6, 14]. When limited trip information is available, optimal EMS can be implemented by assuming that the velocity is constant for that horizon [16]. This novel EMS strategy could be implementable in-vehicle controllers with an MPC type of framework.

In the sub-sequent sections, I extensively studied previous research studies on optimal EMS and quantified and compared the fuel economy improvement by utilized a dynamics programming, model predictive control, and constant velocity prediction strategy.

1.1 Literature Review

Starting in 2008, the earliest and presently most cited research pertaining to perception, optimal EMS planning, and FE results comes from researchers at the University of Florida and the University of Wisconsin-Milwaukee. Their study used V2I and GPS signals as inputs into an artificial neural network (NN) perception model, and FE improvements using an Optimal EMS in a PHEV were realized [17]. In 2013, researchers at the University of Stuttgart, Germany integrated a perception model and a planning model. The planning optimal EMS only determines the optimal time to implement the hydraulic power [18]. In 2014, researchers at the University of Minnesota applied a traffic model to

predict future vehicle velocity with V2V and V2I as inputs [19]. They employed Pontryagin's minimization principle to derive their Optimal EMS and realized a 1.5% to 4.5% FE improvement with prediction-with-error scenario. Then in 2015, researchers from the University of California at Berkeley recognized the important relationship between perception and planning and investigated three perception models for use with a Model Predictive Control Optimal EMS. They used previous driving data and the current vehicle state as inputs to test an exponentially varying perception model, a stochastic Markov chain perception model, and an NN perception model [20]. Their results show that the NN perception model with model predictive control as the Optimal EMS produced the best FE results, though this result was not a full realization of globally optimal FE.

Starting in 2017, researchers at Colorado State University began publishing research that included a perception model, optimal EMS, and FE results [references]. The first study used current and previous vehicle velocity and GPS data input to a shallow NN perception model with an Optimal EMS computed using DP on a validated model of a 2010 Toyota Prius. The maximum FE improvement of x% was achieved using 30 seconds of prediction [21]. Another follow-up study used custom camera detections relevant for velocity prediction [7], travel time data, as well as current and previous vehicle velocity and GPS data as the sensor/signal inputs again with a shallow NN and an Optimal EMS [22]. Additionally, research that was conducted at the University of Michigan and then transitioned to Western Michigan University explored a variety of perception models including auto-regressive moving average, shallow NN, long short-term memory (LSTM) deep NN, markov chain, and conditional linear gaussian models. It was determined that the LSTM deep NN provided the best prediction fidelity (measured in mean absolute error) [23] which realized a fuel economy improvement of 3% in a dynamometer validated model of a 2017 Toyota Prius Prime [24].

Recent trends have begun to implement advancements in machine learning and have replaced shallow NNs with deep NNs. This was first demonstrated by researchers at the University of California Riverside where a deep reinforcement network was implemented as a perception and planning subsystem where traffic data was the input and optimal control of a generic PHEV was the output. This technique resulted in a 16.3% FE improvement in simulation [25].

1.2 Motivation

In terms of global energy consumption, the transportation sector is the second largest consumer behind the industrial sector. Transportation accounts for 30% of the world's energy consumption and the transportation energy demand is projected to increase 30% from current levels by 2040 [3]. Associated utilization of energy conversion devices such as the internal combustion engine, result in issues spanning climate stability, domestic energy security, and human health risks from local air quality impacts. The global transportation sector accounted for 64.5% of worldwide petroleum consumption in 2014 [3]. As a 2016 estimation shows that the United States alone paid $150 billion to the Organization of Petroleum Exporting Countries (OPEC), which creates issues like energy insecurity and vulnerability to geopolitical instability. The transportation sector is also a major contributor to air pollution. Out of the six primary air pollutants, transportation significantly contributes to worldwide nitrogen oxide/nitrogen dioxide (NOx), carbon monoxide (CO), volatile organic compounds (Voc), particulate matter (PM), and sulfur dioxide (SO2) [3]. As a result, 6.5 million premature deaths were attributed to air pollution in 2012, making it the world's fourth-largest threat to human health [12]. Greenhouse gas emissions resulted in increased climatic changes and the transportation sector was also responsible for 23% of global greenhouse gas emissions in 2014 [6]. To combat these climate impacts, the Paris climate agreement has been adopted by most countries to limit greenhouse gas emissions and with the goal of keeping global warming to at most 2ºC [6]. Limiting greenhouse gas emissions from transportation is proposed to be accomplished primarily through the increasing of fuel economy (FE) with technologies such as improved vehicle operation efficiency and electrification [2, 6].

Overall, increasing vehicle FE (reducing petroleum consumption), results in lower global energy consumption, lower greenhouse gas emissions, and lower air pollution emissions. Automotive FE standards, such as those adopted by the United States, Japan, Canada, Australia, China, Taiwan, South Korea, and others, have proven to be one of the most effective tools in controlling petroleum demand and greenhouse gas emissions in many regions and countries around the world [6]. There are three types of vehicle controls that reduce fuel consumption for a drive cycle with a fixed starting point and a fixed ending point: (1) Eco-Driving, (2) Eco-Routing, and (3) an improved Energy Management Strategy

(EMS). Eco-Driving and Eco-Routing decreases fuel consumption by decreasing the energy output of the vehicle through modification of the drive cycle. An improved EMS decreases fuel consumption by increasing the efficiency of the vehicle powertrain operation without modification of the drive cycle.

Eco-Driving reduces fuel consumption for all types of vehicles by implementing fuel efficient driving behaviors along a fixed route which may alter the travel time. In practice, Eco-Driving is challenging to implement because most drivers do not like to give up control [6]. On the other hand, Eco-Routing reduces fuel consumption for all types of vehicles by exploring alternate vehicle routes between a fixed starting and ending location. As vehicles become more intelligent, Eco-Routing can assist vehicles in real time [6].

An improved EMS seeks to reduce the energy consumption over a fixed drive cycle through improved powertrain operation efficiency. Typically, an optimal control problem is formulated and an Optimal Energy Management Strategy (Optimal EMS) is derived. An Optimal EMS realizes FE improvements by explicitly or implicitly modeling vehicle operation and controlling the vehicle powertrain components to minimize fuel consumption. An Optimal EMS does not require a change in driver behavior; thus, this FE improvement technique has a consumer acceptance advantage over Eco-Driving and Eco-Routing. An Optimal EMS can realize FE improvements for conventional vehicles and electric vehicles, but the greatest FE improvements are realized from vehicles with more powertrain operation degrees of freedom such as HEVs and PHEVs. The exact FE improvement from an Optimal EMS is strongly dependent on the chosen drive cycle and vehicle architecture. As an example, one of the earliest Optimal EMS studies demonstrated a 28% FE improvement in a hybrid electric truck through optimal control of the gear shifting and battery charging and discharging [6]. Quantifying FE improvement through various Optimal EMS is the focus of this thesis research.

1.3 Optimal Energy Management Strategies

Developing and implementing an Optimal EMS has most commonly been posed as an application of optimal control [6]. A mathematical optimization problem is formulated by defining a dynamic equation which describes the current state of the vehicle, a cost function

that penalizes using fuel and any other variables of interest, and constraints that ensure a desired final value of the battery state of charge is met, powertrain component limitations are not violated, and that the drive cycle is fixed. This optimization problem is also described in equations as follows:

Dynamic Equation:

$$\text{New Battery State of Charge} = f(\text{Battery State of Charge, Engine Power, velocity})$$

Cost Equation:

$$\text{Cost} = \text{Sum}(\text{mass of fuel used})$$

Constraints:

- Desired battery state of charge at the end of drive cycle.
- Powertrain component physical limitations
- Fixed drive cycle.

This framework can be utilized as either a second by second instantaneous optimization, or as a global optimization which includes future vehicle operation prediction. The solution from either of these schemes is the minimum fuel consumption strategy (or Optimal EMS) which can be then be applied to operate the vehicle powertrain.

1.3.1 Instantaneous optimal EMS

An instantaneous Optimal EMS involves finding the optimal control strategy that minimizes fuel consumption at the instant in time for which sampled data is available. In PHEVs such as the Toyota Prius Prime and the Chevrolet Volt, studies [references] using an instantaneous Optimal EMS have led to the "charge-depleting, charge-sustaining" EMS, where all excess battery power is used first, then the battery charge is sustained afterwards.

1.3.2 Predictive Optimal EMS

A predictive Optimal EMS involves finding the optimal control strategy that minimizes fuel consumption for the window of time in which prediction data is available. Figure 1 represents the general working principle of PHEV, where both engine and battery pack provide the total required power to run the vehicle. On the other hand, energy management in HEV means deciding the amount of power delivered by both energy sources at each instant to achieve desired vehicle velocity.

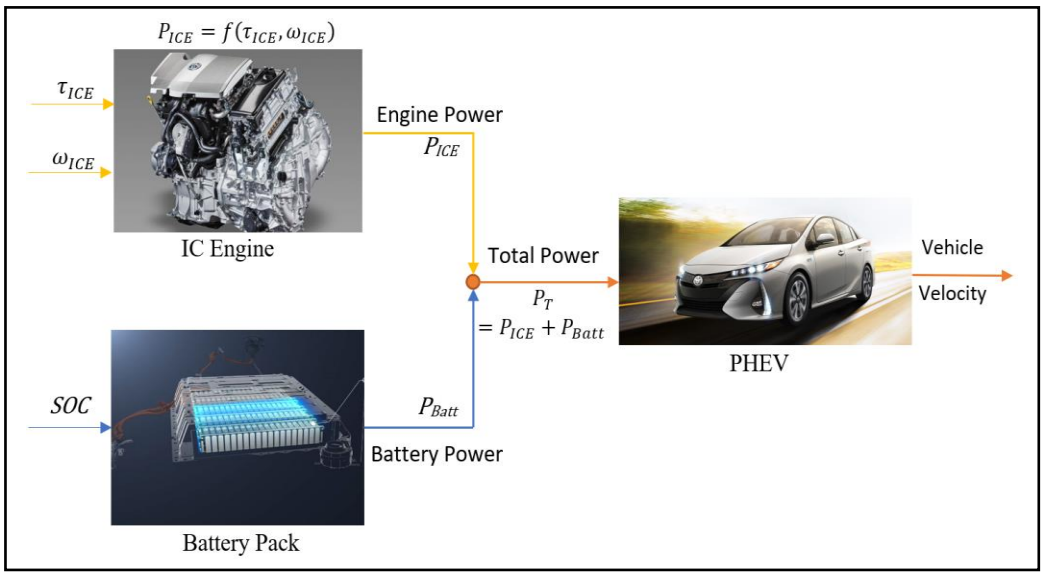

Figure 1. General Working Principle of HEV

Figure 2 represents the principle of predictive optimal EMS. If it is assumed that the desired vehicle speed and desired acceleration, as well as road grade are known for the entire duration of the optimal control problem, i.e., the DC. From the desired speed and acceleration, the total desired power at each time instant can be computed. Given the total desired power, the required IC engine power can be determined for each candidate value of the control inputs engine torque and engine speed. Also, this engine torque values, together with engine speed, determine fuel consumption rates. The fuel consumption rates typically make up the costs in the choice of power split ratios at each time step. The SOC of the battery also needs to be determined for each choice of power split ratio, in order to ensure that upper and lower constraints on SOC are not violated.

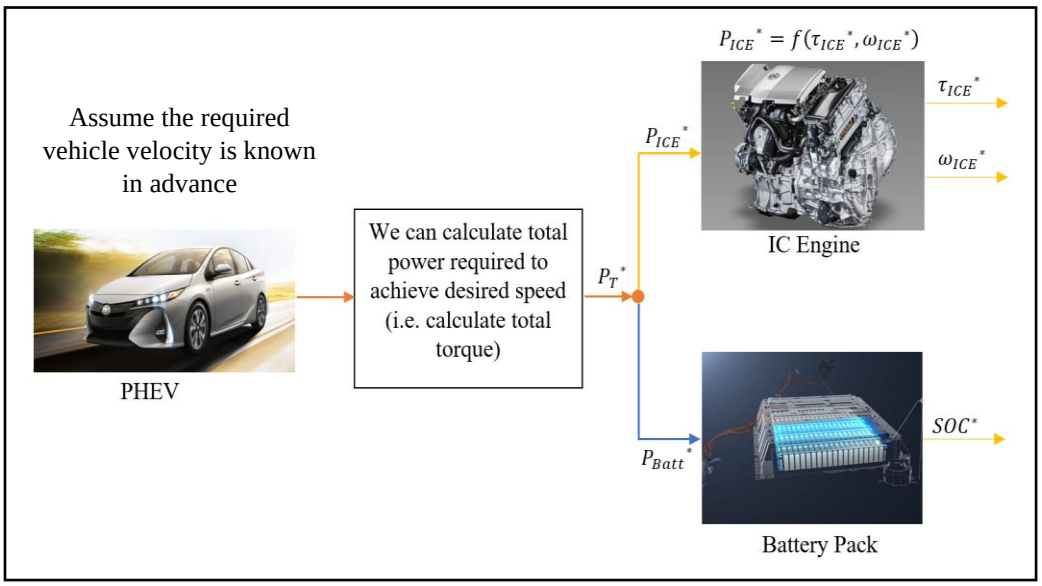

Figure 2. Predictive Optimal Energy Management Strategy Principle

The systems-level viewpoint of predictive optimal EMS is composed of four subsystems as shown in Figure 3: a vehicle perception subsystem, a vehicle planning subsystem, and a vehicle plant subsystem which includes a vehicle running controller. The input to the Optimal EMS system is a variety of sensors that detect environmental information, thus defining vehicular surroundings (commonly referred to as the worldview in autonomous vehicle literature). This worldview can be used to generate a prediction of future vehicle states through artificial intelligence, stochastic modeling, regression analysis, and more. The vehicle state prediction can then be utilized in a mathematical optimization problem to determine powertrain operation that maximized FE. The maximum FE powertrain operation is then issued as a request to the vehicle running controller, which enforces component constraints and may be subject to various disturbances such as future vehicle state prediction error. The powertrain operation from the running controller is actuated in the vehicle plant, and the FE or energy consumption can be measured.

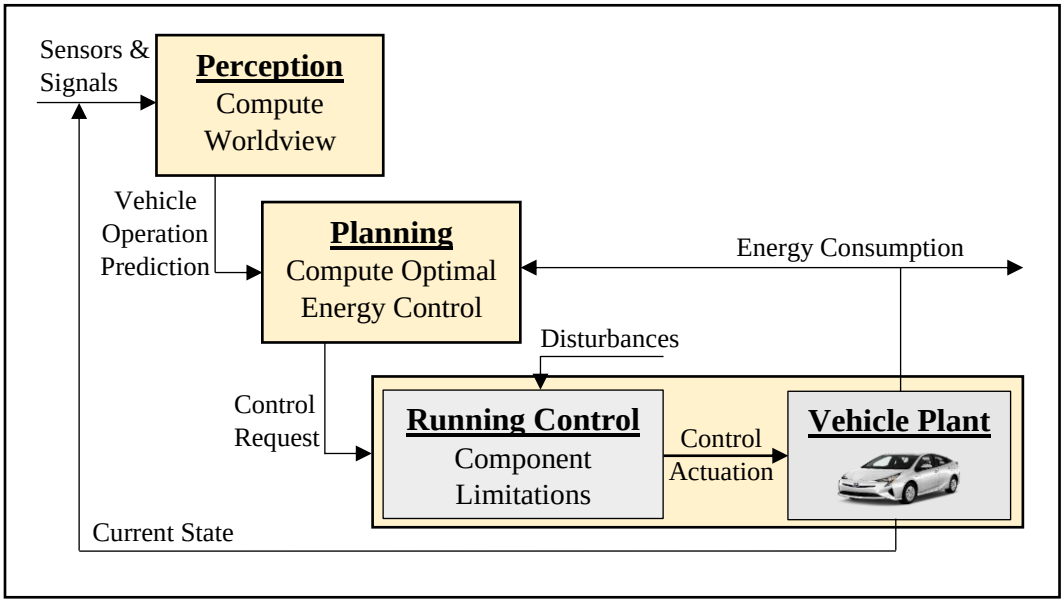

Figure 3. Detailed View of Predictive Optimal Energy Management Strategy [6]

1.3.2.1 Perception

The perception subsystem receives sensor and signal inputs, defines vehicle surroundings, and thus computes future vehicle operation as an output. The input data to the predictive optimal EMS is a series of sensors and signals such as CAN data, RADAR, GPS, V2V, V2I, and traffic data which recognize environmental information, thus defining vehicular surroundings. This can be used to produce a forecast of future vehicle states through a deep neural network, stochastic modeling, regression analysis, and more [23,24].

1.3.2.2 Planning

The planning subsystem receives the vehicle operation prediction as an input and computes the optimal control as an output. Note that the planning subsystem is only required to compute the optimal control and issue a control request, this subsystem is not tasked with achieving the optimal control in the vehicle; achieving the optimal control is accomplished with the vehicle running controller.

1.3.2.2.1 Globally Optimal EMS with Deterministic Prediction

A globally Optimal EMS with deterministic prediction is derived using either dynamic programming (DP) or pontryagin's minimization principle (PMP) which is based on

calculus of variations [6]. When deriving a globally Optimal EMS using deterministic prediction, DP has been the overwhelming favorite of researchers due to its ease of use, robustness, and that no derivatives or analytic expressions are required [6]. A globally Optimal EMS with deterministic prediction is difficult to implement in practice because of the high computational cost but it is still beneficial in simulation to define the upper practical limit on FE benefits for a given vehicle and drive cycle.

1.3.2.2.2 Optimal EMS with Stochastic Prediction

An Optimal EMS with stochastic prediction is used in applications where researchers are willing to forgo a guarantee of global optimal FE in favor of a robustness to stochastic prediction errors. In other words, stochastic derivation strategies are appropriate for applications where a small increase in FE over a wide range of drive cycles is desired. Stochastic derivation strategies include stochastic dynamic programming (SDP) [6] and adaptive equivalent consumption minimization strategy (a-ECMS) [13].

1.3.2.2.3 Computationally Limited Optimal EMS to Enable Practical Implementation

Computationally limited practical implementation Optimal EMS also forgoes the guarantee of global optimal FE in favor of computationally efficient algorithms that can be used in current and near future vehicles. Practical implementation derivation strategies in current vehicles include optimized rules-based control [6], equivalent consumption minimization strategy (ECMS) [6], and model predictive control (MPC) using fast optimizers.

1.3.2.3 Running Controller and Vehicle Plant

The final subsystem is comprised of the vehicle running controller and the vehicle plant which receives the optimal control request and the current vehicle state as inputs, determines physically feasible vehicle operation that does not violate torque, battery state of charge, speed, acceleration, etc. limits and actuates the vehicle plant thus producing vehicle movement and a measurable FE or energy consumption as outputs.

1.4 Optimal EMS Developed in This Research

As explained in literature study, limited study is done previously which address globally optimal EMS with perfect full DC prediction, computationally efficient non-global optimal with perfect horizon prediction and limited perception. The methods I used in my research to address the above is as follows:

1.4.1 Dynamic Programming

When deriving a globally optimal EMS using deterministic prediction, DP has been the overwhelming favorite due to its ease of use, robustness, and no need for derivatives required. A globally optimal EMS with deterministic prediction is difficult to implement in practice because of the high computational cost but it is still beneficial in simulation to define the upper limit on FE benefits for a given vehicle and drive cycle

1.4.2 Model Predictive Control

For computationally efficient non-global optimal EMS model predictive control (MPC) can be implement, where the optimization is done over a moving finite horizon that is shorter than the DC. Also, with the advancement in perception systems and associated computational improvements, MPC could be implementable in real vehicles [6, 26]

1.4.3 Constant Velocity Prediction

When limited trip information available, we can implement optimal EMS by assuming the current velocity is constant over the current horizon [16]. This novel EMS strategy could be implementable in-vehicle controllers within an MPC framework.

1.5 Hybrid-Electric Vehicles

HEVs and PHEVs are unique in that they have two sources of vehicle propulsion energy available. These vehicles can be powered from either battery power, engine power, or a combination of both. This additional operational degree of freedom unlocks the potential for improved overall powertrain efficiency with intelligent control strategies. Examples of how this increased vehicle powertrain operational freedom can be used to reduce fuel consumption include regenerating energy during braking, storing excess energy from the

engine during coasting, and modifying the power-split powertrain component operation for maximum efficiency [16]. There are mainly 3 types of powertrains seen in hybrid-electric vehicles are as follows -

1.5.1 Parallel Hybrid Powertrain

As the name suggests itself, in a parallel hybrid powertrain IC engine and electric machines are placed in parallel to the transmission and ultimately to the vehicle wheels, as shown in Figure 4. Both the energy sources can simultaneously provide power to the wheels using a suitable transmission system. As there is no engine power to electric power conversion that happens in the parallel hybrid powertrain, it works with higher efficiency as power conversion losses get nullified. However, the major drawback of this system is, IC engine cannot operate at its optimal operation region. Instead, it works over wide operation region to fulfill the vehicle power demand. The battery gets recharged by the electric motors during regenerative braking.

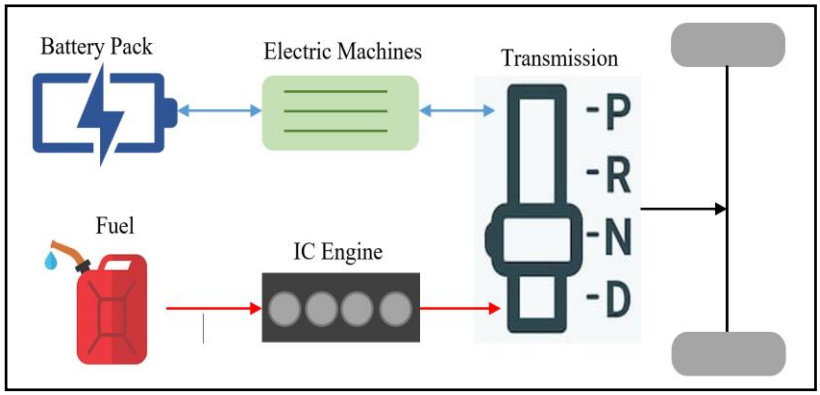

Figure 4. Parallel Hybrid Electric Vehicle Architecture Layout [16]

1.5.2 Series Hybrid Powertrain

As the name suggest, in a series hybrid powertrain, the IC engine, battery, and electric machines are placed serially to the vehicle wheels. As Figure 5 shows, the IC engine is not directly connected to the vehicle wheels. Instead, it got connected to the battery pack through the generator. In series hybrid powertrain, the only power source is in direct connection with the wheels is the electric motor. The power is provided either by the battery-pack or by the engine-generator to the motor to drive the wheel. In this system, engine can

work in its most optimal operating region as it is not directly connected to the wheels, so engine does not need to work over a wide operation range. As this system can efficiently work with smaller engines, which could also reduce the engine cost. But on the other hand, to fulfill the required demand, it may need a larger battery pack than parallel hybrid powertrain, which ultimately increases the cost of the overall system. The battery can be recharged both from the engine-generator set and from the motor during regenerative braking. In regenerative braking, motor acts as a generator and recharges the battery [16]

.

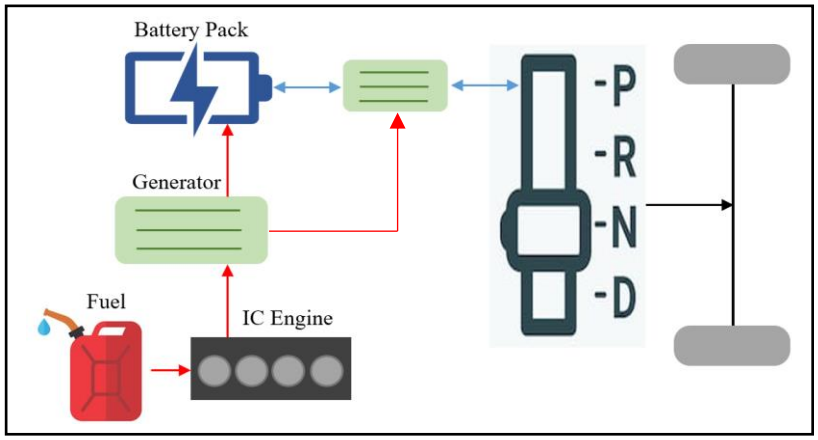

Figure 5. Series Hybrid Electric Vehicle Architecture Layout [16]

1.5.3 Series-Parallel Hybrid Powertrain

As the name suggests, the series-parallel hybrid powertrain combines the benefits of both series and a parallel hybrid powertrain. In this system, both the energy sources can run the vehicle wheels simultaneously like parallel hybrid powertrain and work as a series hybrid powertrain by disconnecting the wheels from the engine and run only by an electric motor, as shown in Figure 6. We can also split the engine power and provide one part directly to the wheels and another part to the motor through the generator set. By doing this, we can set the engine operation in its most optimal operative range. In low-speed operation, it works as a series hybrid because of stop-and-go driving nature. On the other hand, at high-speed operation, it works as a parallel hybrid with higher efficiency as the mechanical to electric conversion losses get nullified as the engine is now directly connected to the wheels. The battery can be recharged by the engine-generator set or by a motor during regenerative braking. Also, we can split the engine power to drive the wheels and to recharge the battery

using excess engine power. The Toyota Prius is a common example of a hybrid vehicle that consists of a power-split hybrid powertrain. [16]

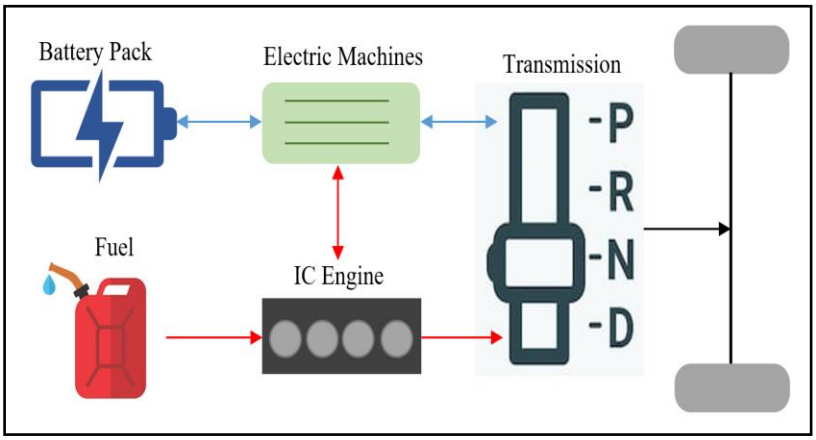

Figure 6. Series-Parallel Hybrid Electric Vehicle Architecture Layout [16]

1.6 Novel Contribution

The novel contribution of my research are as follows:

- Use of DP, MPC, and constant velocity prediction to quantify the fuel economy improvements
- Use of control-oriented, high-fidelity vehicle model
- Use of high-fidelity DP optimizer with MPC
- Development of "Constant Velocity Prediction" strategy
- Use of high-fidelity DP optimizer with constant velocity prediction strategy.
- Effect analysis of discretization steps, interpolation methods on FE improvement

2. HIGH-FIDELITY, CONTROL-ORIENTED VEHICLE MODEL

2.1 Toyota Prius Prime Model into MATLAB

Toyota created the modern hybrid car segment in 1997 with the debut of the original Prius. Over the last 22 years, it remains one of the important hybrid cars in its class due to its efficiency, blends of technology, and usability. Toyota Prius Prime is a new generation of Toyota PHEV, where the primary difference from the previous PHEV system is that the new version has a one-way clutch between the engine and the planetary gear-set, which could step-up electric propulsive force with the help of generator [27]. Because of these reasons, I selected a 2017 Toyota Prius Prime vehicle to demonstrate the potential FE improvements of the Optimal EMS. This high-fidelity, controls-oriented model was developed using previously documented Toyota Prius operation equations implemented with MATLAB/Simulink to calculate different types of vehicle performance, especially fuel economy and battery state [25].

(Note – Due to confidentiality clause, I'm not able to disclose exact vehicle parameters.)

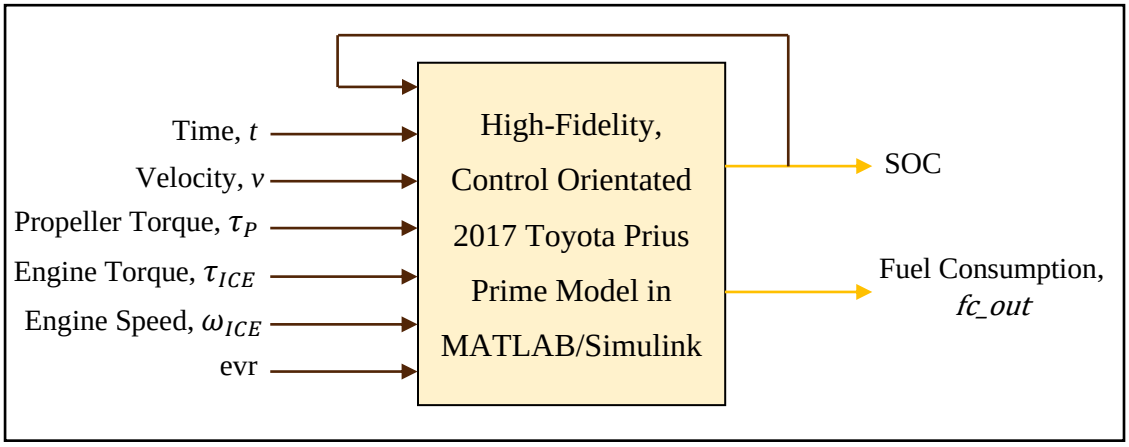

Figure 7. Overview of High-Fidelity, Control-Oriented Vehicle Model

Figure 7 shows the block diagram of overall vehicle model. The input to the vehicle model is predicted vehicle velocity (v), propeller torque (τ_P), engine torque (τ_{ICE}), engine speed (ω_{ICE}), next state of battery at each time-step. Figure 8 shows examples of input parameters versus. distance traveled. As mentioned earlier the output of the model is fuel consumption and battery state of charge at the end of a time-step. As shown in the block

diagram, the calculated SOC is a feedback into the model because it is a dynamic variable. The detailed model components are explained in further sections,

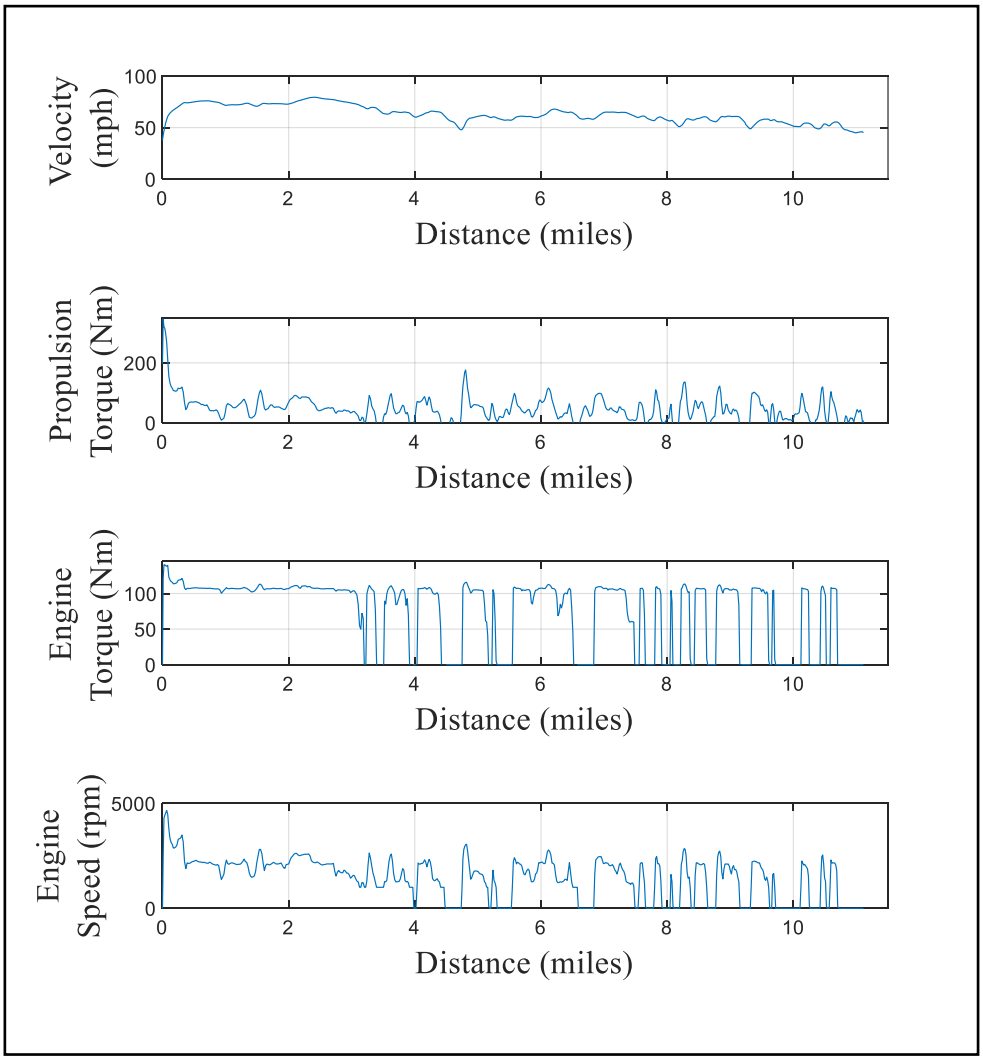

Figure 8. Input Parameters Vs. Distance Graph

While model development I kept accessary power zero, and ev ratio one,
$P_{acc} = 0$, $evr = 1$.

Where,

$$evr = \frac{Motor\ Direct\ Torque}{Motor\ Direct\ Torque + Generator\ Direct\ Torque}$$

- **Calculation of Engine Fuel consumption**

As the primary goal in HEV is to minimize fuel consumption, which can be calculated with an engine map at different operating conditions. If we know the engine

torque and engine speed, we can find the fuel consumption rate using an engine map. A contour on the map represents a constant fuel consumption contour for a range of torque and engine speed conditions. A 2-D lookup table is widely used to represent the engine map. Where engine torque and engine speed represent rows and columns, respectively. If the operating point is in between the grid points, then linear interpolation can be used to find the fuel consumption at that operating point [10, 16].

- **Calculation of Next State of Charge**

To take the advantages of both parallel and series hybrid powertrains, Toyota Prius used planetary gear system in their power-split architecture as shown in Figure 9 to provide engine torque to both vehicle wheel and to a generator to recharge the battery [10, 16].

The planetary gear system shown in Figure 10, the engine is connected to the carrier gear, a generator to the sun gear, common shaft of motor and wheel to the ring gear by a reduction gear. It is possible to connect the engine to both generator and wheels by using pinion gears [10, 16]. The total torque required to run the vehicle is a summation of ring gear torque and the torque produced by the electric motor as per equation 1.

$$(\omega_s\, R_s) + (\omega_r\, R_r) = \omega_c\, (R_s + R_r) \quad \text{.....1}$$

where, R_s, R_r are radii of the ring and sun gear respectively, and ω_s, ω_r, ω_c are rotational speeds of sun, ring and carrier gears respectively.

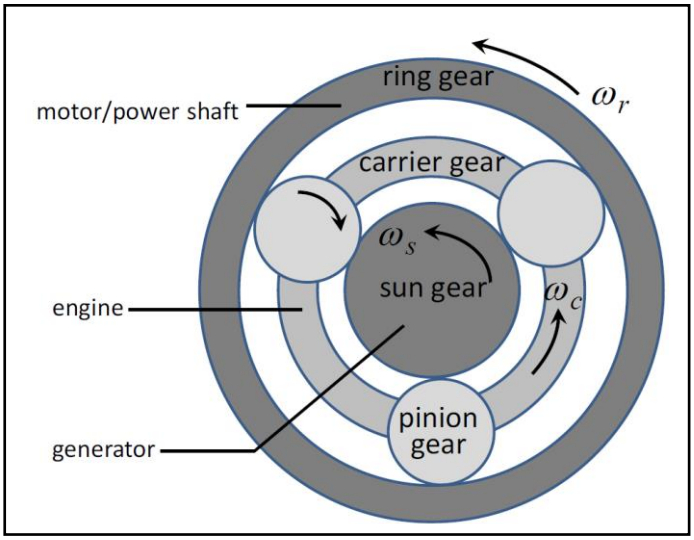

Figure 9. Planetary Gear System [16]

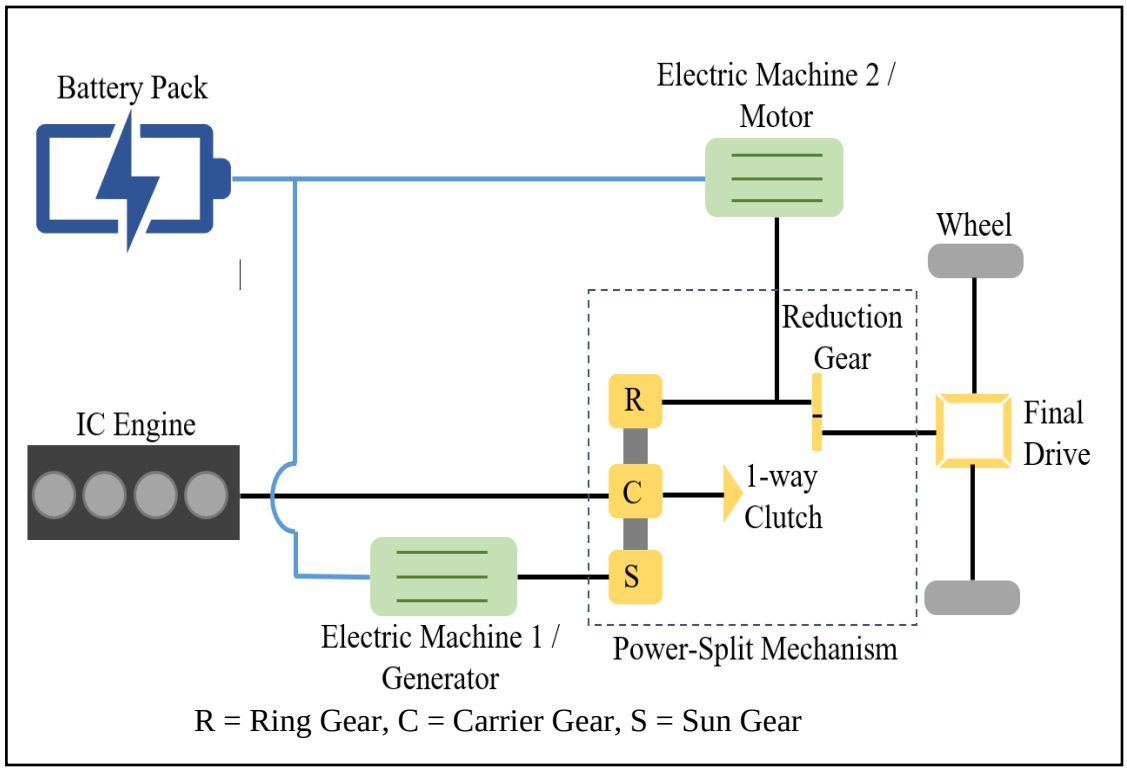

Figure 10. Power-Split Architecture with Planetary Gear Train Arrangement [27]

- Electric Machine 1 / Generator Model:

Due to the addition of one-way clutch at the engine side and planetary gear set in power-split hybrid structure, engine can provide torque to both the wheels as well as to the electric machine 1/generator. The generator is connected to the sun gear which charges the battery [10, 16].

When engine speed is equal to 0 and propeller torque is positive (battery provides power), the vehicle is propelled by both electric machines [10, 16]. The relation between generator, motor, engine and wheel torque is as follows –

$$\tau_G = -(\rho \times \tau_P \times (1 - evr)) \quad \text{.....2}$$

$$\tau_M = (\tau_P \times (evr/Grm)) \quad \text{.....3}$$

On the other hand, when engine speed is positive, and vehicle is also driven by traction motor the relation between generator, motor, engine and wheel torque is as follows –

$$\tau_G = -\tau_{ICE} \times \left(\frac{\rho}{1+\rho}\right) \quad \text{.....4}$$

$$\tau_M = \frac{\left(\tau_P - \left(\frac{\tau_{ICE}}{1+\rho}\right)\right)}{Grm} \quad \text{.....5}$$

where,
τ_G = Electric Machine1 or Generator Torque.
τ_M = Electric Machine1 or Motor Torque.
ρ = Gear ratio between sun gear and the ring gear = $\frac{R_S}{R_r}$
Grm = motor gear ratio.

As in the Toyota Prius Prime, the vehicle wheels are connected to the ring gear through a reduction gear. The rotational speed of the ring gear is given as follows –

$$\omega_r = \left[v \times \left(\frac{1}{R_t}\right) \times G_r\right] \quad \text{.....6}$$

As the generator is connected to the sun gear, the rotational speed of sun gear is equal to the generator speed ($\omega_s = \omega_G$). From Equation 1, the generator speed is,

$$\omega_G = \left[\omega_{ICE} \times \left(\frac{1+\rho}{\rho}\right)\right] - \left(\frac{\omega_r}{\rho}\right) \quad \text{.....7}$$

The motor and ring gear are on same shaft and wheels are connected to the ring gear through a reduction gear. Motor speed and ring gear speed are proportional:

$$\omega_M = \left(\frac{\omega_r}{Grm}\right) \quad \text{.....8}$$

where,
R_t = wheel radius
G_r = final reduction gear ratio.
V = Vehicle Speed
ω_r = Rotational Speed of Ring gear (rpm).
ω_G = Generator Speed (rpm).
ω_M = Motor Speed (rpm).

- Battery Model/ Battery Dynamics:

Power discharge from the battery to the motor and charging from the generator to the battery is given by [10, 16],

$$P_{Batt} = P_G + P_M + P_{acc} \quad \text{.....9}$$

Where,
P_{Batt} = Battery Power.
P_G = Generator Power.
P_M = Motor Power.

The generator and motor power are calculated using torque and speed of generator and motor respectively as follows –

$$P_G = \left[\tau_G \times \omega_G \times \left(\frac{2\pi}{60}\right) \times \left(\frac{1}{1000}\right)\right] + G_{coreloss} \quad \text{……..10}$$

$$P_M = \left[\tau_M \times \omega_M \times \left(\frac{2\pi}{60}\right) \times \left(\frac{1}{1000}\right)\right] + M_{coreloss} \quad \text{……..11}$$

where, the $G_{coreloss}$ and $M_{coreloss}$ are generator core-loss and motor core-loss respectively. This electrical loss are function of torque, speed and open circuit voltage of generator and motor respectively.

- A contour generator core-loss and motor core-loss map provides both the core losses at different torque, speed and open circuit voltage.
- The values of core losses at operating points between the grid points in the matrix are obtained by interpolation.
- $Generator\ Coreloss = f(\tau_G, \omega_G, V_{OC})$
- $Motor\ Coreloss = f(\tau_M, \omega_M, V_{OC})$

Also, battery power can be calculated from the electrical dynamics of the battery system as follows –

$$P_{Batt} = \left[(V_{OC} * I_{Batt}) - \left(R_{Batt} * {I_{Batt}}^2\right)\right] \text{……12}$$

Where,
V_{OC} = Open Circuit Voltage.
I_{Batt} = Battery Current.
R_{Batt} = Battery Resistance.

As I already calculated the battery power using equation 13, and other parameters can be calculated as follows -

Open Circuit Voltage Calculation:

The open circuit voltage (V_{OC}) means the battery voltage when it is not connected to any load is a battery characteristic and is mainly a function of battery state of charge and battery temperature. Consider battery temperature is 25℃.

- A contour V_{oc} map provides V_{oc} at different SOC and battery temperature.
- The values of V_{oc} at operating points between the grid points in the matrix are obtained by interpolation.
- $V_{oc} = f(SOC, T_{Batt})$

Where,
T_{Batt} = Battery Temperature.

Battery Resistance Calculation:

As of the open circuit voltage, battery resistance is also a battery characteristic and is mainly a function of battery state of charge and battery temperature [10, 16].

Consider battery temperature is 25℃.

- A contour R_{Batt} map provides R_{Batt} at different SOC and battery temperature.
- The values of R_{Batt} at operating points between the grid points in the matrix are obtained by interpolation.
- $R_{Batt} = f(SOC, T_{Batt})$

By rearranging equation 13,

$$\left(R_{Batt} * {I_{Batt}}^2\right) + (V_{OC} * I_{Batt}) - P_{Batt} = 0 \quad \text{.....13}$$

Equation 13 becomes a quadratic equation in the form of I_{Batt}. So, we can calculate battery current by solving this quadratic equation as follows -

$$I_{Batt} = \frac{V_{OC} - \sqrt{{V_{OC}}^2 - (4 \times P_{Batt} \times R_{Batt})}}{2 \times R_{Batt}} \quad \text{.....14}$$

But this battery current doesn't account the constant voltage current loss of battery. So, again calculate battery current by considering constant battery voltage current losses as follows-

$$P_{Batt,vcl} = P_{Batt} + VC_{loss}$$

Where, VC_{loss} is the battery voltage current loss. which is function of battery current, and open circuit voltage.

- A contour Voltage Current Loss map provides Voltage Current Loss at different battery current and open circuit voltage.
- The values of Voltage Current Loss at operating points between the grid points in the matrix are obtained by interpolation.
- $R_{Batt} = f(I_{Batt}, V_{OC})$

Now, calculate battery current with all losses as follows -

$$I_{Batt,final} = \frac{V_{OC} \pm \sqrt{{V_{OC}}^2 - (4 \times P_{Batt,vcl} \times R_{Batt})}}{2 \times R_{Batt}} \quad \text{.....15}$$

Using state of charge dynamics, rate of change of SOC can be calculated as follows –

$$\frac{d}{dt} SOC = -\frac{I_{Batt,final}}{Q_{Batt}} \quad \text{.....16}$$

Where,
Q_{Batt} = total/maximum charge of fully charged battery.

Finally, state of charge of next state is calculated as follows –

$$SOC(k+1) = SOC(k) + \left(\frac{d}{dt}SOC\right) \quad \text{.....17}$$

Again, for the next step calculations provide this calculated SOC as a one of the inputs. Figure 11 shows the example outputs (fuel consumption and SOC) of the developed high-fidelity, control-orientated HEV model. Figure 11(a) and 11(b) shows model outputs means SOC and cumulative fuel consumption with respect to distance graphs. In the highlighted section of Figure 12(a), Y point represents SOC at respective distance, and it also shows that I successfully developed chare-sustaining, control-oriented model.

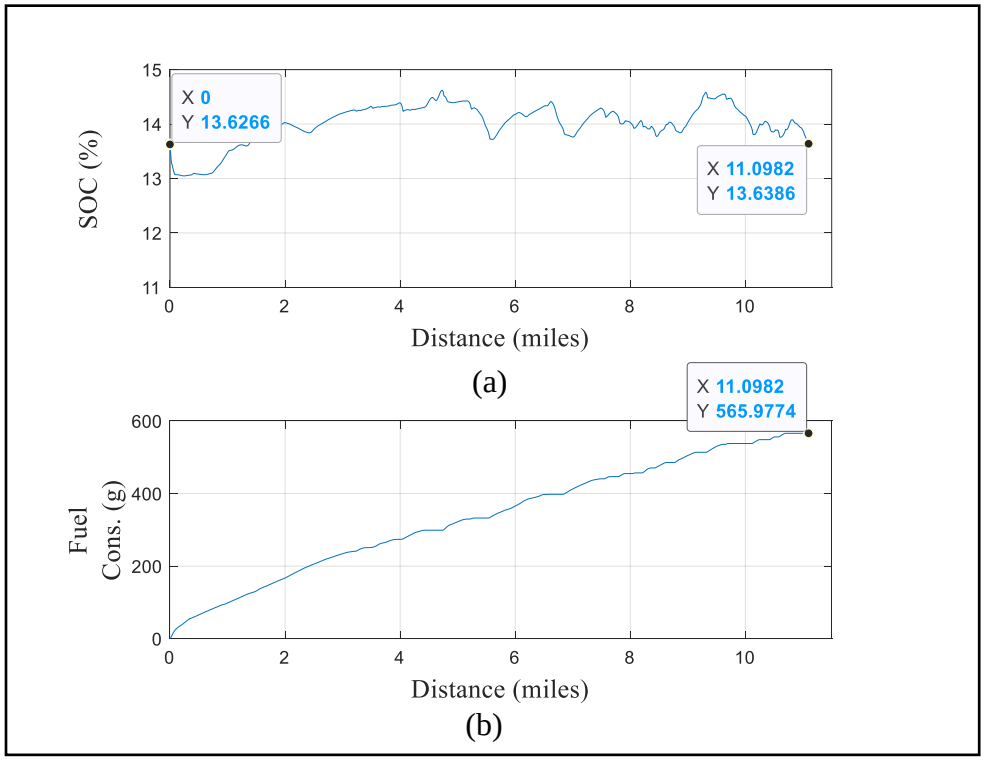

Figure 11. Output Parameters Vs. Distance Graph

2.2 Model Validation

Comparison and validation between the controls-oriented model used in this research and chassis dynamometer data are shown in Figure 12-13 where Figure 12 is fuel consumption and Figure 13 is the initial SOC_i at the beginning of the DC and the final SOC_f at the end of the DC. These plots show a linear relationship between this control-oriented

model and the chassis dynamometer data for both fuel consumption and *SOC* across the industry-standard U.S. Environmental Protection Agency (EPA) drive cycles, including the Urban Dynamometer Driving Schedule (UDDS) and Highway Fuel Economy Test (HWY), and more. Because there is a linear relationship between the control-oriented model and chassis dynamometer data over a variety of standard drive cycles, the model is considered to be validated [24].

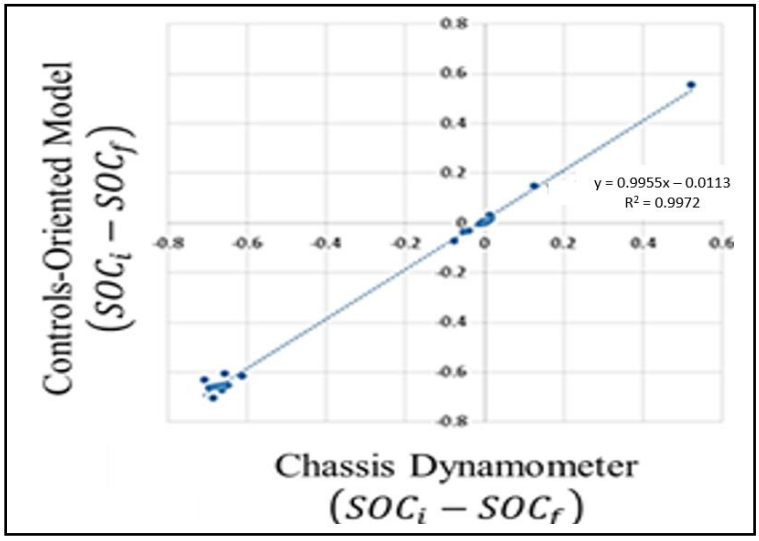

Figure 12. A Comparison Between the Controls-Oriented Model Used in this Research and Chassis Dynamometer Data of Fuel Consumption

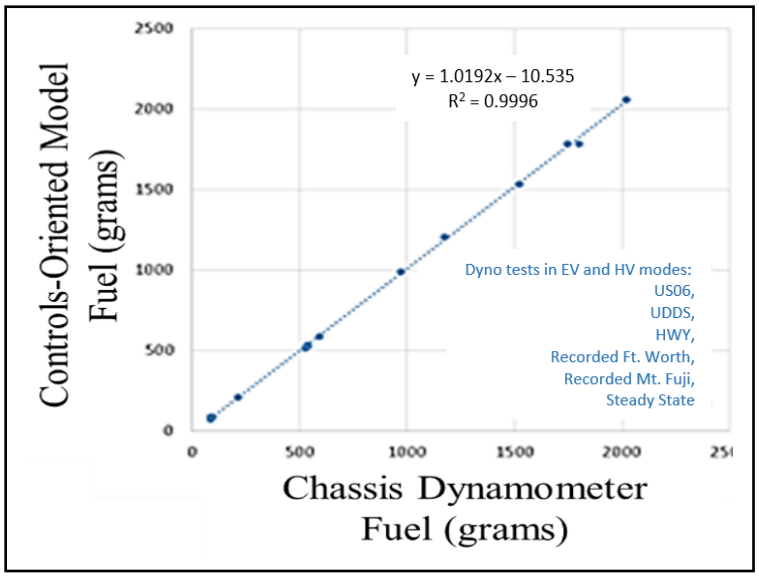

Figure 13. The Initial SOC_i at the Beginning of the DC and the Final SOC_f at the End of the DC

3. OPTIMAL ENERGY MANAGEMENT STRATEGIES

3.1 Grid Convergence Study and the Effect of Interpolation Method

Before presenting the optimal EMS, it is very important to discuss the effect of discretization steps and the interpolation method used in the optimal EMS development. Here we assumed the accessory power is zero. In Figure 14 from a to d we step by step discretized the control and state variables more finely. In all Figures X-axis represents interpolation methods available and Y-axis represents the FE improvements numbers. The very first 2 Figures i.e. with coarse grid and medium grid, the effect of interpolation methods shows significant effect on FE improvement results. That make difficult to decide which interpolation method to use in the simulations. As we move downward from a→b→c→d the effect of interpolation methods got nullified after a certain state (from c). The effect of interpolation methods faded away as we make the grid size finer and finer. Also, it gives us freedom to select any of the interpolation method. So, in our research while developing the optimal EMS we utilized the control and state variables discretization steps as Figure 14-c.

S	**1**
u_1	10
u_2	200

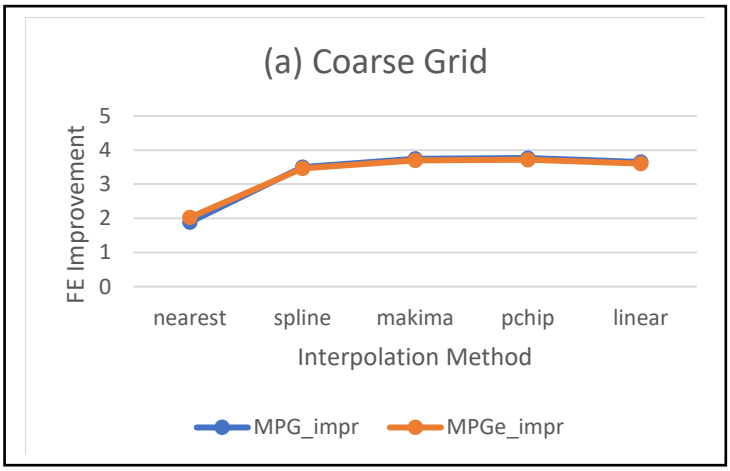

S	**0.5**
u_1	5
u_2	50

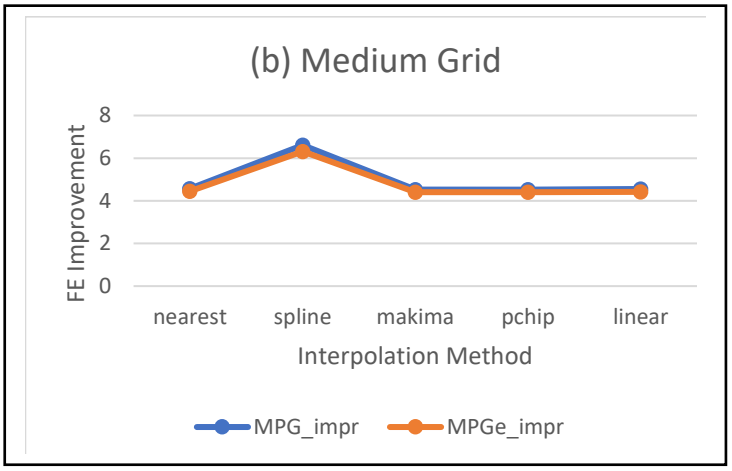

S	**0.1**
u_1	1
u_2	10

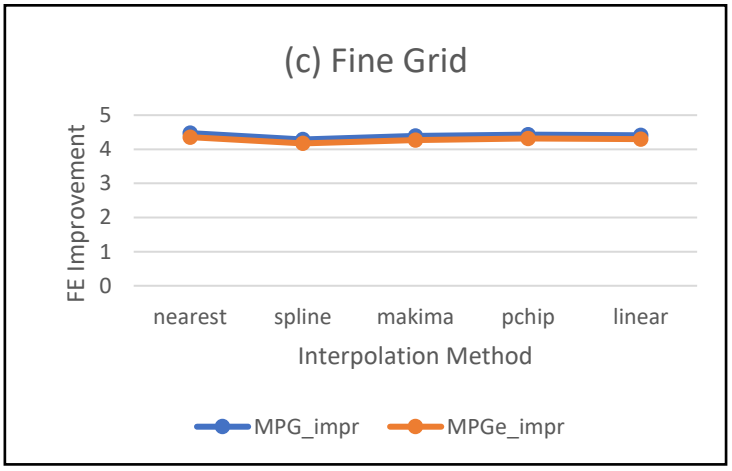

S	**0.01**
u_1	0.5
u_2	5

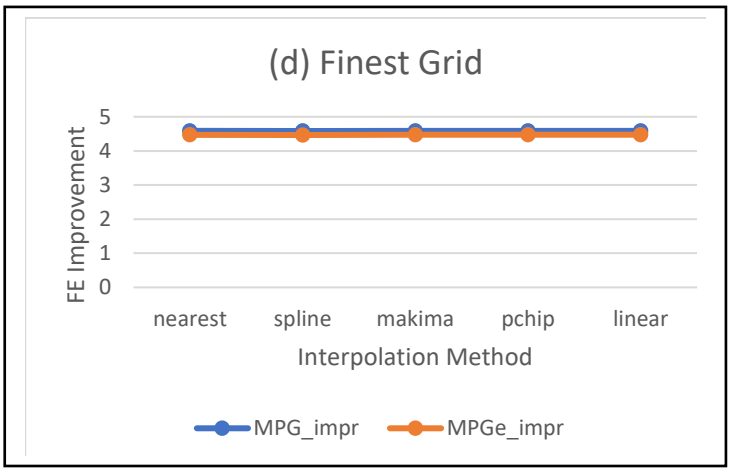

Figure 14. Grid Convergence and Interpolation Method Effect.

3.2 Dynamic Programming

Based on Bellman's principle of optimality, DP is a numerical method, which is applicable to multistage decision-making problems like Optimal EMS. It finds the global optimal solution by working backward in time [9, 31, 32]. We assumed that the desired future speed of the entire DC is obtained from the perception sub-system. To solve any problem with DP, first the dynamic equation and the cost function must be discretized. This can be done most conveniently by dividing the total DC time into N equal interval of Δt. So, time can be expressed as $t = k\,\Delta t$ where k is time index. The predicted speed data can be used to calculate the total desired power and subsequently the optimal control (engine torque and engine speed) values that deliver the desired IC engine power [15, 16]. Fuel consumption rates are calculated based on these data along with IC engine speed. Whereas, *SOC* of battery is also calculated at each power-split ratio and each time index to make sure it doesn't violate the SOC constraints.

The detailed DP planning sub-system is shown in Figure 15. It takes future velocity as an input to calculate optimal controls by proceeding backward in time and provides optimal EMS decision matrix consisting of optimal control matrix to calculate optimal engine power, SOC and fuel consumption at optimal EMS section [24]. Figure 16 shows the principle of backward recursive DP optimization, where it takes full DC prediction as an input and apply DP optimizer backwards to calculate optimal control and next state.

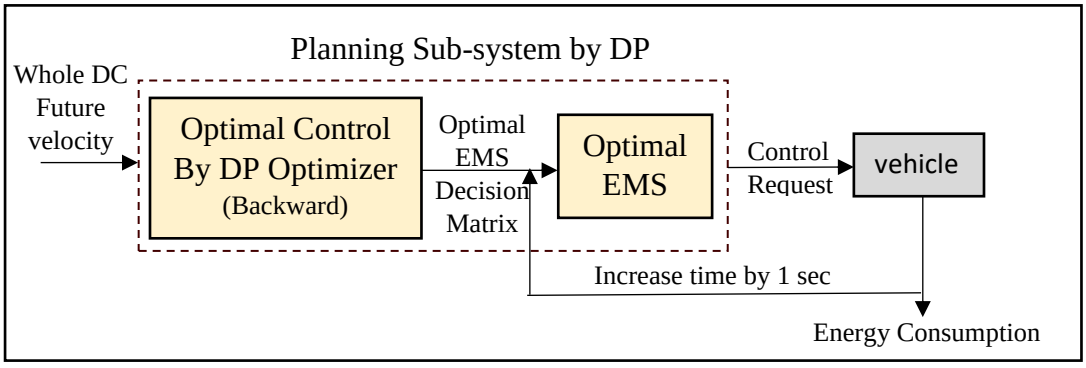

Figure 15. Detailed View of Planning Sub-System by DP

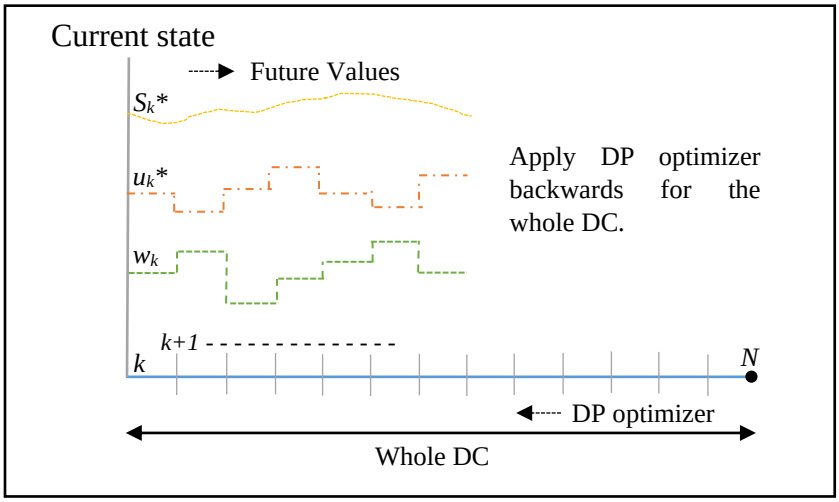

Figure 16. Working Principle of Dynamic Programming

In general, the DP technique consists of a dynamic equation, a cost function (*J*), state (*S*) and control variables (*U*) with feasibility constraints. In our study, we implemented DP on a 2017 Toyota Prius Prime by setting SOC as a state variable (*S*), engine speed (u_1) and engine torque (u_2) as a control variables, vehicle velocity as an exogenous input (*w*) and the summation of mass of fuel used and charge sustaining penalty as a cost function which is to be minimized.

The overall DP formulation given by equation 17 is as follows

Dynamic Equation:

$$s(k+1) = f(s, u_1, u_2, w_1, w_2, k)\Delta t \quad \text{.....18}$$

The simplified DP equation consisting - all dynamic equations of vehicle, battery, motor, and generator of power-split architecture with planetary gear train arrangement is,

$$s(k+1) = s(k) - C_1 + \sqrt{C_2 - \left[C_3 \times u_2 \times \left((C_4 \times u_1) - (C_5 \times w_1)\right)\right] - \left[C_6 \times w_1 \times \left((C_7 \times w_2) - (C_8 \times u_2)\right)\right]} \quad \text{.....19}$$

Where, *k* is time index, *SOC(k)* is current SOC, *SOC(k+1)* is derived next SOC after applying control, *C* values are constant used to display the equation in a simple way (please refer appendix).

Cost Function

The cost function is the summation of the addition of mass of fuel used and charge

sustaining deviation penalty.

$$Cost = m_{fuel}(u_1, u_2) + W\left(SOC_f - SOC_{f,\ Baseline\ EMS}\right)^2 \ldots\ldots\ldots\ldots\ldots\ldots\ldots 20$$

where - m_{fuel} is mass of fuel used which is a function of engine speed and engine torque derived using engine map. W is a penalty weight (1665 - 1670), $SOC_{f,\ Baseline\ EMS}$ is the final SOC of baseline EMS.

Constraints

$$s_{min}(k) \le s(k) \le s_{max}(k) \equiv 10\% \le SOC(k) \le 20\%$$
$$u_{1min}(k) \le u_1(k) \le u_{1max}(k) \equiv 0Nm \le \tau_{ICE}(k) \le 140Nm$$
$$u_{2min}(k) \le u_2(k) \le u_{2max}(k) \equiv 0rpm \le \omega_{ICE}(k) \le 5200rpm$$

Optimal Control Formulation by DP

Start with defining inputs like all vehicle constants, and exogenous inputs. Here we considered vehicle velocity, v and propulsion torque, τ_P as our inputs w_1, and w_2 respectively.

Then we defined the state vector, $\vec{s}$ and discretized with a step of δs from a minimum value of s_{min} to a maximum value of s_{max} as follows –

$$\vec{s} = \{s_{min}, s_{min} + \delta s, \ldots\ldots s_{max}\}$$

The same we did for control variables $\vec{u}_1, \vec{u}_2$ as follows

$$\vec{u}_1 = \{u_{1min}, u_{1min} + \delta u_1, \ldots\ldots u_{1max}\}$$

$$\vec{u}_2 = \{u_{2min}, u_{2min} + \delta u_2, \ldots\ldots u_{2max}\}$$

Where, $\delta s = 0.01\%$, $\delta u_1 = 1$Nm, and $\delta u_2 = 10$ rpm. Also, the length of $\vec{s}, \vec{u}_1, \vec{u}_2$ vectors are N_s, N_{u_1}, and N_{u_2} respectively.

Now make a 3-D matrix of $\vec{s}, \vec{u}_1, \vec{u}_2$ for simplicity and to reduce computational time. So, the new control and state variables are,

$$S = [s]_{\vec{s},\vec{u}_1,\vec{u}_2}$$
$$U_1 = [u_1]_{\vec{s},\vec{u}_1,\vec{u}_2}$$
$$U_2 = [u_2]_{\vec{s},\vec{u}_1,\vec{u}_2}$$

Now evaluate the vehicle model by backward recursive dynamic programming to calculate next state and fuel consumption.

for k = N, N-1, ... 1

Now simulate the vehicle model described in previous section from equation 1 - 19 calculate the next state and cost function at each grid point of state and control variables for given constraints.

$$S(k+1) = f(S, U_1, U_2, w_1, w_2)\Delta t$$

While calculating the cost, keep in mind that we assumed charge sustaining mode i.e $S(k+1) = S(k)$. So, arrangements were made where, if this condition gets violated, then apply a penalty on that to keep final state equal to the first as follows,

if $Sk+1 > Sf, BaselineEMS$

$$Cost = m_{fuel}(U_1, U_2)$$

else

$$Cost = m_{fuel}(U_1, U_2) + W(SOC_f - SOC_{f,\ Baseline\ EMS})^2$$

end

Now extract a minimum/optimal cost for each state and at each time index in the form of matrix $J^*[k, \vec{s}]$. Also, find out the index of minimum cost ($I_{min\ cost}$) to find the control value associated with each minimum cost. For each admissible state and time, the control index that generates the optimal cost is stored in the matrix $u_1{}^*\ [k, \vec{s}\ ]$, *and* $u_2{}^*\ [k, \vec{s}\ ]$ *as follows* –

$$J^*[k, \vec{s}] = minimum\ (Cost[\vec{s}, \vec{u}_1, \vec{u}_2])$$

$$u_1{}^*\ [k, \vec{s}\ ] = U_1(I_{\min cost})$$

$$u_2{}^*\ [k, \vec{s}\ ] = U_2(I_{\min cost})$$

end

3.3 Model Predictive Control

Even though DP gives globally optimal EMS, it is also very difficult to implement in practice because full DC cannot be predicted currently. Nowadays many researchers are exploring the optimal EMS which can be implemented practically. Model predictive control

(MPC) is a prospective strategy that can deliver optimal controls with practical considerations [22, 33, 34, 35, 36].

Model predictive control (MPC) involves control of a dynamic system based on different control inputs which are applied from the current time to a future time resulting in minimization of a cost function subject to the system dynamics and additional constraints [37, 38, 39]. The detailed MPC planning sub-system is shown in Figure 17 and the working principle of MPC is shown in Figure 18.

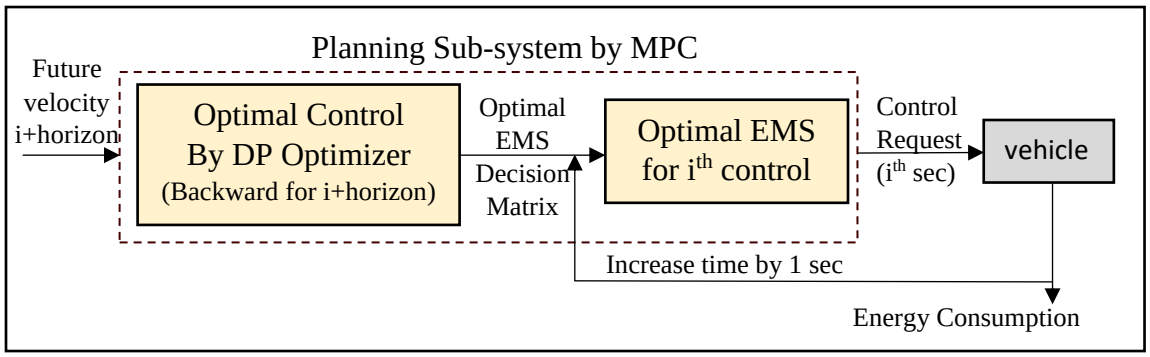

Figure 17. Detailed View of Planning Sub-System by MPC

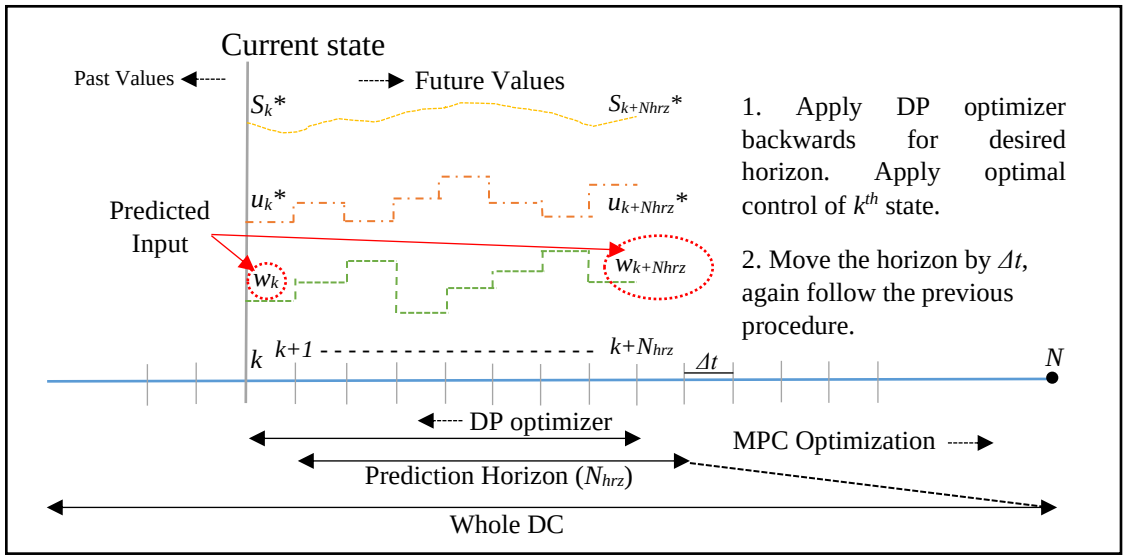

Figure 18. Working Principle of Model Predictive Control

As we don't know the whole DC prediction in advance, we only know the velocity predictions for the desired horizon at each time index as we move forward. So, it takes the predicted velocity of the desired horizon as an input to calculate optimal controls only for that selected horizon using DP optimizer in backward in time. This process provides us

optimal control for the entire horizon. But for further optimal EMS calculation just select the controls of the desired time index.

In general, MPC consists of a control equation, a cost function (*J*), state (*S*) and control variables (*U*) with feasibility constraints. In our study, we have implemented MPC with a 10-second prediction horizon and keeping DP as the optimizer. The overall MPC formulation for 2017 Toyota Prius Prime model is as follows

Control Equation:

$$s(k+1) = f(s, u_1, u_2, w_1, w_2, k)\Delta t \quad \ldots\ldots\ldots\ldots\ldots\ldots\ldots\ldots\ldots\ldots\ldots\ldots\ldots\ldots 21$$

where - *k* is time index, *SOC(k)* is current SOC, *SOC(k+1)* is derived next SOC after applying control, u_1 is engine speed, u_2 is engine torque, w_1, w_2 are an exogenous input - velocity, and propulsion torque respectively.

Cost Function: The cost equation is the same as DP. Only the difference is considered only horizon time, not whole DC.

$$Cost = m_{fuel}(u_1, u_2) + W\left(SOC_f - SOC_{f,\ Baseline\ EMS}\right)^2 \ldots\ldots\ldots\ldots\ldots\ldots 22$$

Constraints: constraints are also the same as one used in DP. Only consider for the horizon.

$$s_{min}(k) \le s(k) \le s_{max}(k) \equiv 10\% \le SOC(k) \le 20\%$$
$$u_{1min}(k) \le u_1(k) \le u_{1max}(k) \equiv 0Nm \le \tau_{ICE}(k) \le 140Nm$$
$$u_{2min}(k) \le u_2(k) \le u_{2max}(k) \equiv 0rpm \le \omega_{ICE}(k) \le 5200rpm$$

Optimal Control with MPC

To derive optimal controls, DP has been used as an optimizer in MPC. Start with defining inputs like all vehicle constants, and exogenous inputs. Here we considered vehicle velocity, v and propulsion torque, τ_P as our inputs w_1, and w_2 respectively.

Start from 1st time state

for i = 1, 2,……N

Make desired segment of time known as time horizon. Apply DP optimizer only for that horizon, not for the whole DC So, new time and exogenous inputs are $t_{horizon}$, $w_{horizon}$. Then we defined the state vector, $\vec{s}$ and discretized with a step of δs from a minimum

value of s_{min} to a maximum value of s_{max} as follows –

$$\vec{s} = \{s_{min}, s_{min} + \delta s, \ldots . s_{max}\}$$

The same we did for control variables $\vec{u}_1, \vec{u}_2$ as follows

$$\vec{u}_1 = \{u_{1min}, u_{1min} + \delta u_1, \ldots . u_{1max}\}$$

$$\vec{u}_2 = \{u_{2min}, u_{2min} + \delta u_2, \ldots . u_{2max}\}$$

Where, $\delta s = 0.01\%$, $\delta u_1 = 1Nm$, and $\delta u_2 = 10rpm$. Also, the length of $\vec{s}, \vec{u}_1, \vec{u}_2$ vectors are N_s, N_{u_1}, and N_{u_2} respectively.

Now make a 3-D matrix of $\vec{s}, \vec{u}_1, \vec{u}_2$ for simplicity and to reduce computational time. So, the new control and state variables are,

$$S = [s]_{\vec{s},\vec{u}_1,\vec{u}_2}$$

$$U_1 = [u_1]_{\vec{s},\vec{u}_1,\vec{u}_2}$$

$$U_2 = [u_2]_{\vec{s},\vec{u}_1,\vec{u}_2}$$

Now evaluate the vehicle model by applying backward recursive DP optimizer for required time horizon to calculate next state,

for $k = N_{horizon}, N_{horizon} - 1, \ldots . i$

Now simulate the vehicle model described in previous section from equation 1 - 19 calculate the next state and cost function at each grid point of state and control variables for given constraints.

$$S(k+1) = f(S, U_1, U_2, w_{1,horizon}, w_{2,horizon})\Delta t$$

While calculating the cost, keep in mind that we assumed charge sustaining mode i.e. $S(k+1) = S(k)$. So, we made an arrangement where if this condition gets violates then apply a penalty on that to keep final state equal to the first as follows -

if $S_{k+1} > S_{f,\ BaselineEMS}$

$$Cost = m_{fuel}(U_1, U_2)$$

else

$$Cost = m_{fuel}(U_1, U_2) + W(SOC_f - SOC_{f,\ Baseline\ EMS})^2$$

end

Now extract a minimum/optimal cost for each state and at each horizon time index in the form of matrix $J^*[k, \vec{s}]$. Also, find out the index of minimum cost ($I_{min\ cost}$) to

find the control value associated with each minimum cost. For each admissible state and time, the control index that generates the optimal cost is stored in the matrix $u_1{}^*[k,\vec{s}]$, and $u_2{}^*[k,\vec{s}]$ as follows (horizon control matrix) –

$$J_{horizon}{}^*[k,\vec{s}] = minimum\ (Cost[\vec{s},\vec{u}_1,\vec{u}_2])$$

$$u_{1,horizon}{}^*[k,\vec{s}] = U_1(I_{\min cost})$$

$$u_{2,horizon}{}^*[k,\vec{s}] = U_2(I_{\min cost})$$

end

save only 1st results of each $t_{horizon}$ step results to get whole DC control matrix -

$$J_{DC}{}^*[i,\vec{s}] = J_{horizon}{}^*[:,1]$$

$$u_{1,DC}{}^*[i,\vec{s}] = u_{1,horizon}{}^*[:,1]$$

$$u_{2,DC}{}^*[k,\vec{s}] = u_{2,horizon}{}^*[:,1]$$

end

3.4 Constant Velocity Prediction

Due to limitations on perception sub-system, in the near term with limited trip information available or with no trip information available, we can calculate the optimal controls by assuming a constant speed for an assumed finite time horizon [16]. The detailed constant velocity prediction planning sub-system is shown in Figure 19 and the working principle of constant velocity prediction is shown in figure 20.

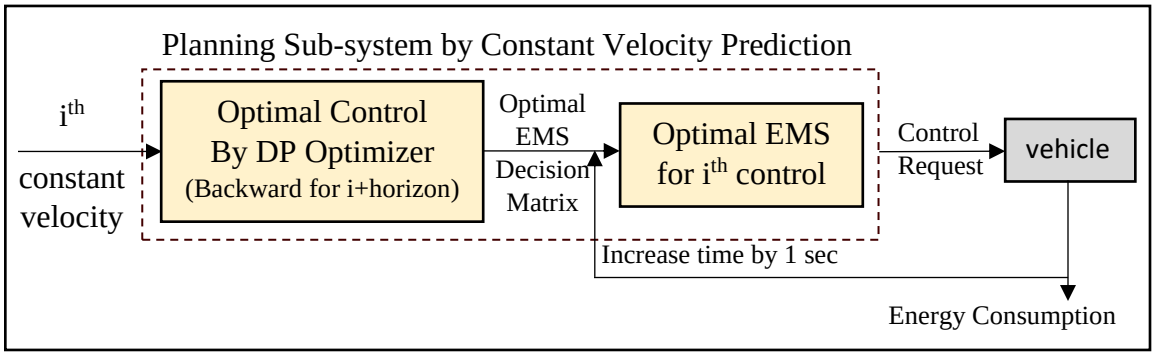

Figure 19. Detailed View of Planning Sub-System by Constant Velocity Prediction

The input to this planning sub-system is the future velocity of an assumed horizon (in our research it is 10 seconds again) as a constant and is equal to the velocity of the current

time-step. The optimal controls for that selected horizon are calculated using DP optimizer moving backward in time. This process provides optimal control for the entire horizon with all horizon velocity same as the current time-step velocity. But for further optimal EMS calculation select the controls which are associated with the current time-step

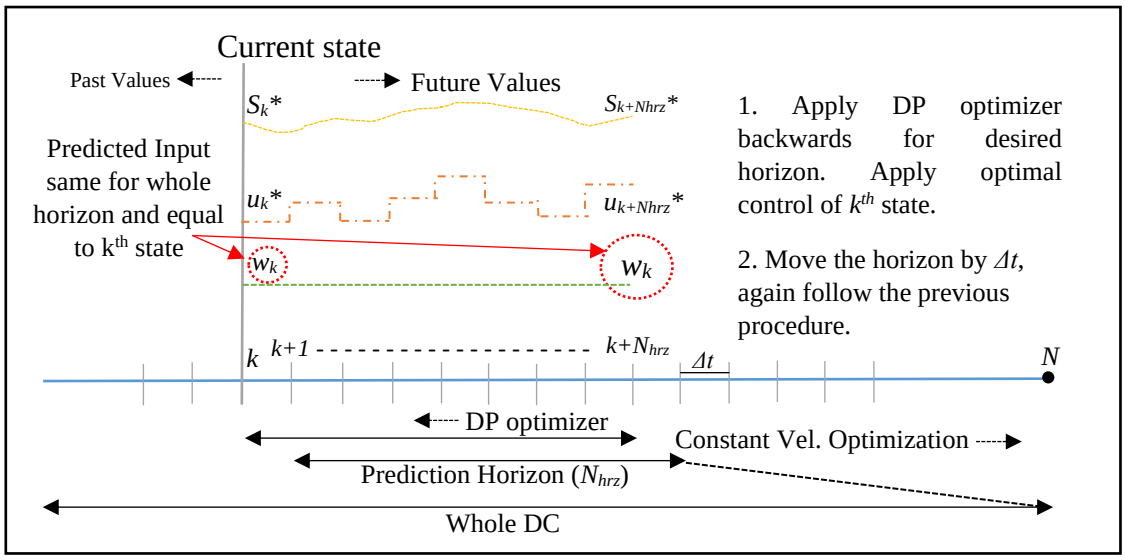

Figure 20. Working Principle of Constant Velocity Prediction

The control equation, cost equation, constraints, state and control variables are the same as previously used in MPC. The only difference is in the horizon velocity.

Optimal Control Formulation by constant velocity prediction

To derive optimal controls, use DP as an optimizer. It starts with defining inputs (all constants, exogenous inputs)

Start from 1st time state

for i = 1, 2,……N

Make desired segment of time known as time horizon. Apply DP optimizer only for that horizon, not for the whole DC by considering i^{th} vehicle velocity as same for whole horizon so, new time and exogenous inputs are $t_{horizon}$, $w_{horizon}$.

Then we defined the state vector, $\vec{s}$ and discretized with a step of δs from a minimum value of s_{min} to a maximum value of s_{max} as follows –

$$\vec{s} = \{s_{min}, s_{min} + \delta s, \ldots\ldots s_{max}\}$$

The same we did for control variables $\vec{u}_1, \vec{u}_2$ as follows

$$\vec{u}_1 = \{u_{1min}, u_{1min} + \delta u_1, \ldots\ldots u_{1max}\}$$

$$\vec{u}_2 = \{u_{2min}, u_{2min} + \delta u_2, \ldots . u_{2max}\}$$

Where, $\delta s = 0.01\%$, $\delta u_1 = 1Nm$, and $\delta u_2 = 10rpm$. Also, the length of $\vec{s}, \vec{u}_1, \vec{u}_2$ vectors are N_s, N_{u_1}, and N_{u_2} respectively.

Now make a 3-D matrix of $\vec{s}, \vec{u}_1, \vec{u}_2$ for simplicity and to reduce computational time. So, the new control and state variables are,

$$S = [s]_{\vec{s},\vec{u}_1,\vec{u}_2}$$
$$U_1 = [u_1]_{\vec{s},\vec{u}_1,\vec{u}_2}$$
$$U_2 = [u_2]_{\vec{s},\vec{u}_1,\vec{u}_2}$$

Now evaluate the vehicle model by applying backward recursive DP optimizer for required time horizon to calculate next state

for k = $N_{horizon}$, $N_{horizon}$ -1, ….i

Now simulate the vehicle model described in previous section from equation 1 - 19 calculate the next state and cost function at each grid point of state and control variables for given constraints.

$$S(k+1) = f(S, U_1, U_2, w_{1,horizon}, w_{2,horizon})\Delta t$$

While calculating the cost, keep in mind that we assumed charge sustaining mode i.e. $S(k+1) = S(k)$. So, arrangements were made where, if this condition gets violated, then a penalty is applied to keep the final state equal to the first as follows –

if $S_{k+1} > S_{f,\ BaselineEMS}$

$$Cost = m_{fuel}(U_1, U_2)$$

else

$$Cost = m_{fuel}(U_1, U_2) + W(SOC_f - SOC_{f,\ Baseline\ EMS})^2$$

end

Now extract a minimum/optimal cost for each state and at each horizon time index In the form of matrix $J^*[k, \vec{s}]$. Also, find out the index of minimum cost ($I_{min\ cost}$) to find the control value associated with each minimum cost. For each admissible state and time, the control index that generates the optimal cost is stored in the matrix $u_1{}^*\ [k, \vec{s}]$, and $u_2{}^*\ [k, \vec{s}]$ as follows (horizon control matrix) –

$$J_{horizon}{}^*[k, \vec{s}] = minimum\ (Cost[\vec{s}, \vec{u}_1, \vec{u}_2])$$

$$u_{1,horizon}{}^{*}\,[k,\vec{s}] = U_1(I_{\min cost})$$

$$u_{2,horizon}{}^{*}\,[k,\vec{s}] = U_2(I_{\min cost})$$

end

save only 1st results of each $t_{horizon}$ step results to get whole DC control matrix -

$$J_{DC}{}^{*}[i,\vec{s}] = J_{horizon}{}^{*}[:,1]$$

$$u_{1,DC}{}^{*}\,[i,\vec{s}] = u_{1,horizon}{}^{*}[:,1]$$

$$u_{2,DC}{}^{*}\,[k,\vec{s}] = u_{2,horizon}{}^{*}[:,1]$$

end

4. SIMULATION

4.1 Drive Cycle on which Data was Collected

Three different instances one of a real-world DC are employed to symbolize highway driving and city-highway driving while simulation to find baseline and optimal FE [23, 24]. The main differences separating these drive cycles are velocities and acceleration through the path. The location of DC's shown in Figure 21 and Figure 22 is in Ann Arbor, MI.

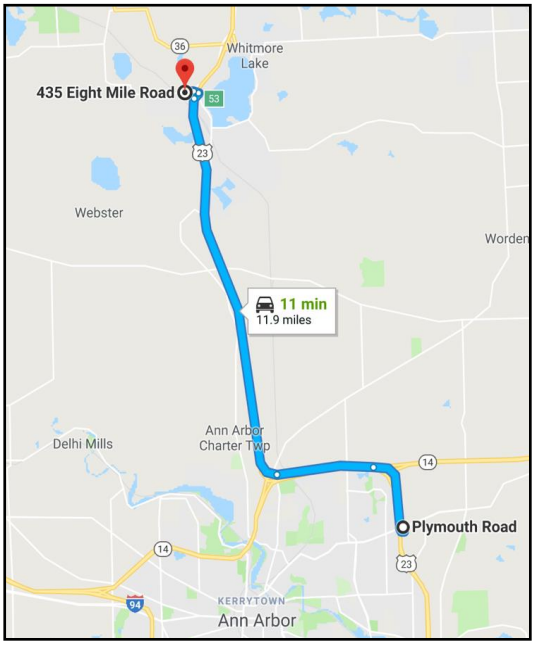

Figure 21. Drive Cycle Map of The Highway Dataset (Created with Google Maps) [23, 24]

Figure 21 shows the DC map of the highway data set and Figure 22 shows the DC map of the city-highway data set created with Google maps. The different instances of each drive cycle may have different traffic conditions and different stop light states along the drive cycle. The total recorded highway DC is 11.9 miles long and city-highway DC is 13.3 miles long.

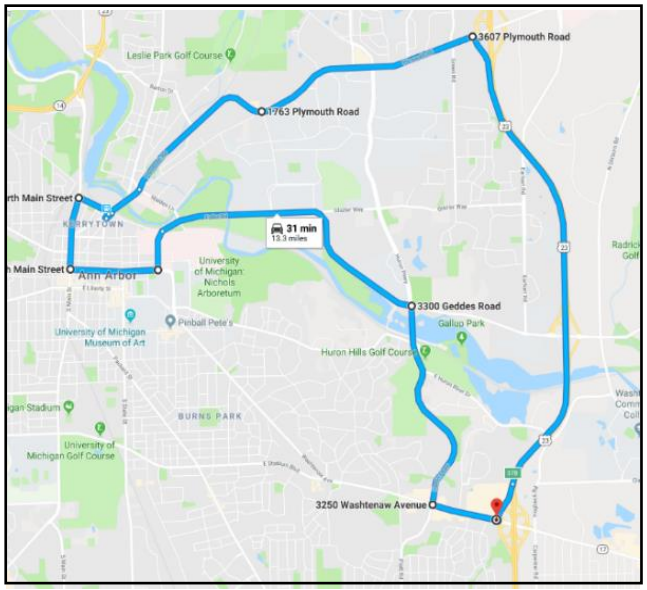

Figure 22. Drive Cycle Map of the City-Highway Dataset (Created with Google Maps) [23, 24]

4.2 Baseline EMS/ Performance

The Baseline EMS represents the current performance of a 2017 Toyota Prius Prime in a rules-based, non-predictive control strategy (due to confidentiality clause, I'm not able to disclose exact rules that used while development). Recorded vehicle velocity, propeller torque, engine speed and engine torque through the whole DC and calculated next state of charge are used as an input into previously developed a controls oriented, high-fidelity HEV model. As mentioned earlier this model was developed using previously documented Toyota Prius operation equations [15, 16]. Integrated with MATLAB/Simulink but updated with vehicle parameters for the engine and motors to accurately represent a 2017 Toyota Prius Prime. Also, in this research, I considered charge sustaining approach. Because charge sustenance and blending incur nearly the same total energy costs through the depletion phase. In blending engine operates efficiently and the battery charge depletes slowly, because in blending engine gets utilized often during the charge depletion phase thereby assisting the battery in meeting total power demand.

Figure 23 and Figure 24 shows the baseline performance of the high-fidelity, control-oriented model with highway and city-highway DC respectively. Figures 23 (a-b-c-d) and 24

(a-b-c-d) represents the velocity, engine power, SOC and cumulative fuel consumption profiles with respect to distance on highway and city-highway DC respectively. Highlighted section of SOC trends from both the figures shows that the developed models achieved charge sustention mode.

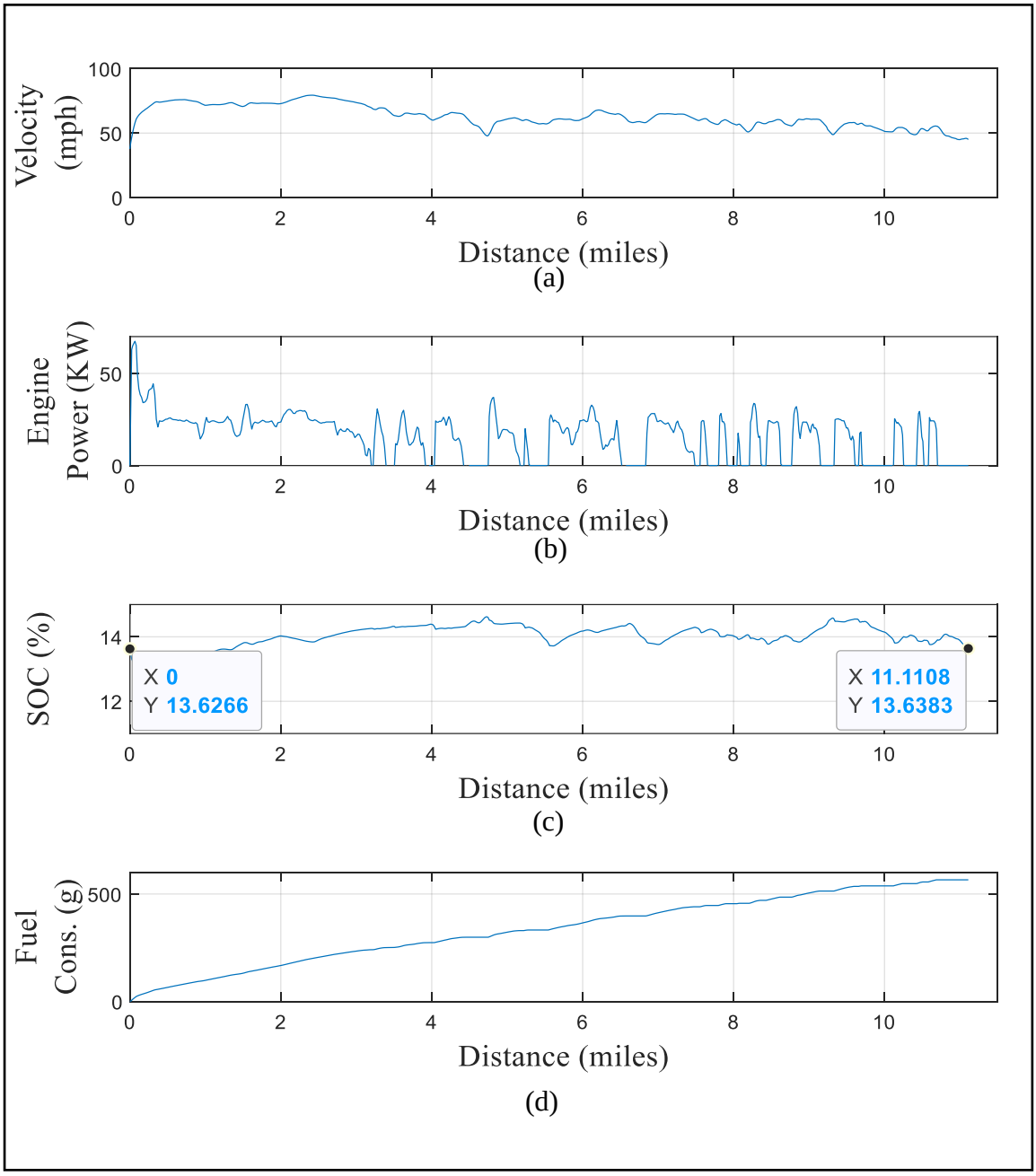

Figure 23. Baseline Performance of High-Fidelity, Control-Oriented Model with Highway DC

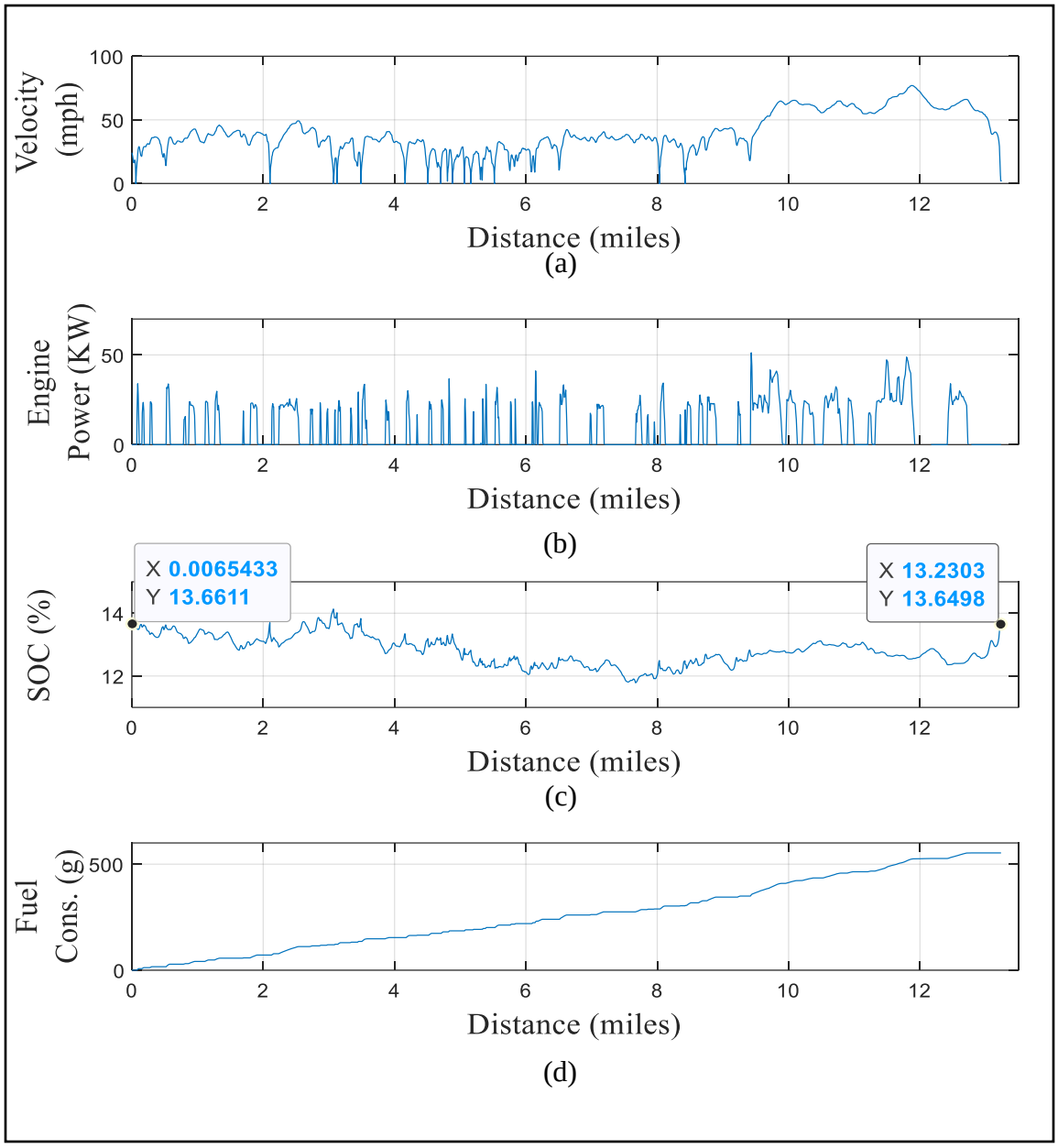

Figure 24. Baseline Performance of High-Fidelity, Control-Oriented Model with City-Highway DC

4.3 Optimal EMS Decision Matrix Using DP

Figure 25 and Figure 26 show the optimal control (u_1* and u_2*) matrix (also called as optimal EMS decision matrix) obtained by full DC prediction using DP with highway and city-highway DC respectively. This plot is 2D representation of 3D graph, where SOC, time

and optimal controls (u_1* and u_2*) are the co-ordinates of 3D graphs. It provides the optimal EMS decision matrix where optimal control is given for each possible value of SOC to achieve desired predicted vehicle velocity. Using this controls the engine power, SOC and fuel consumption has been calculated which is globally optimal.

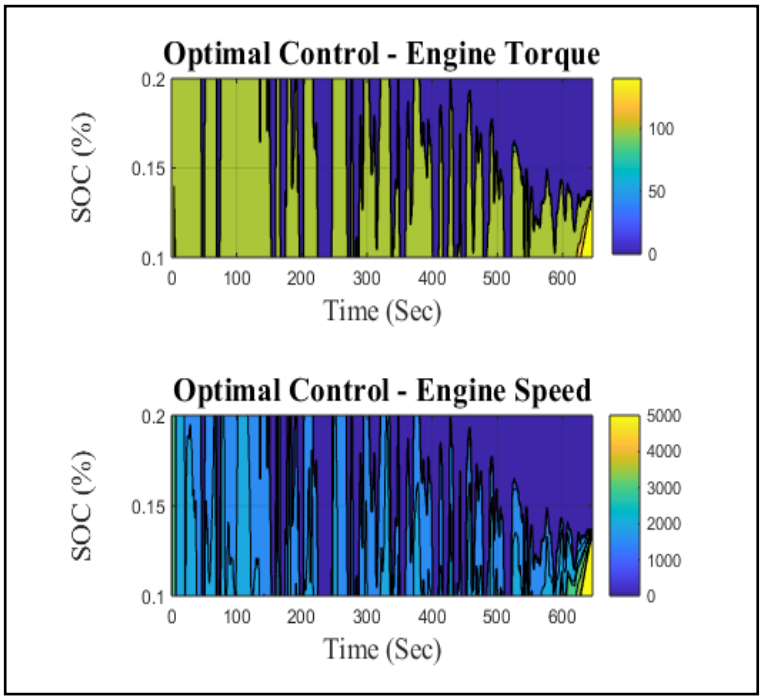

Figure 25. The Optimal Control Matrix Obtained by DP with Highway DC

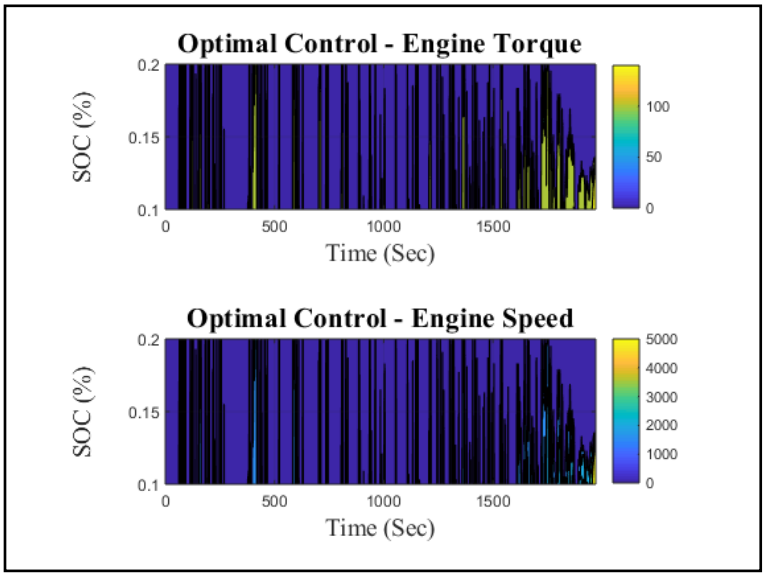

Figure 26. The Optimal Control Matrix Obtained by DP with City-Highway DC

4.4 Optimal EMS Decision Matrix Using 10 sec Horizon MPC

Figure 27 and Figure 28 show the engine power, SOC and fuel-consumption calculated with the optimal control (u1* and u2*) matrix obtained by MPC over a 10 second horizon prediction with highway and city-highway DC respectively.

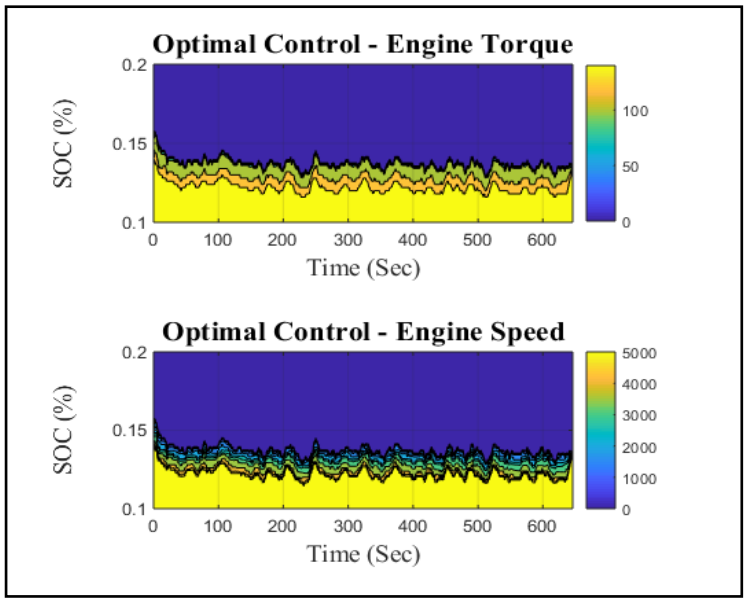

Figure 27. The Optimal Control Matrix Obtained by MPC with Highway DC

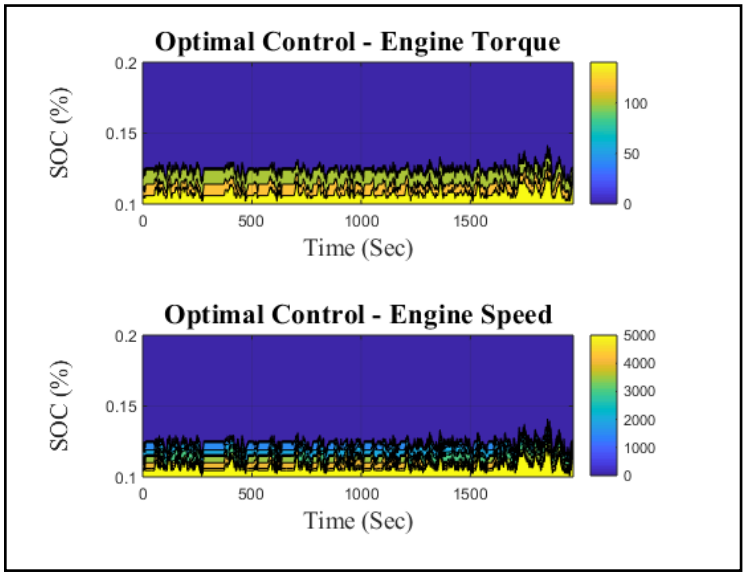

Figure 28. The Optimal Control Matrix Obtained by MPC with City-Highway DC

4.5 Optimal EMS Decision Matrix Using 10 sec Horizon Constant Velocity Prediction

Figure 29 and Figure 30 shows the engine power, SOC and fuel-consumption calculated for the optimal control (u_1* and u_2*) matrix obtained by constant velocity prediction with highway and city-highway DC respectively.

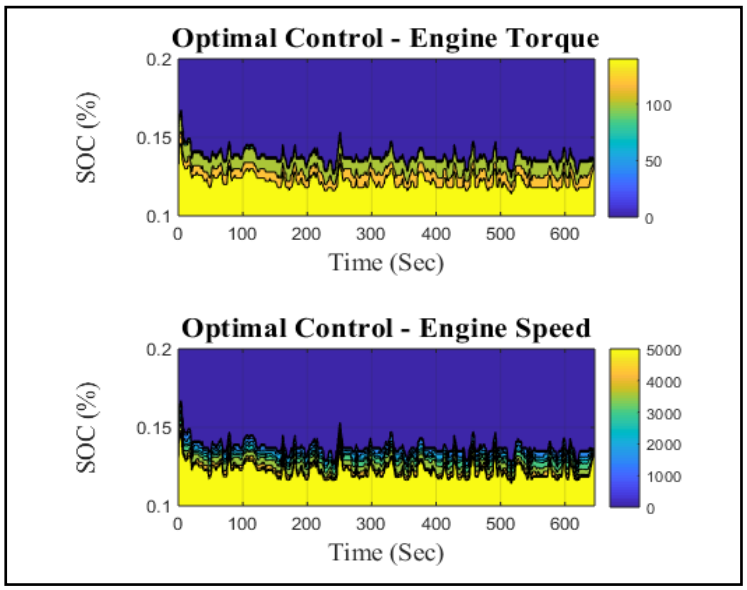

Figure 29. The Optimal Control Matrix Obtained by Constant Velocity Prediction with Highway DC

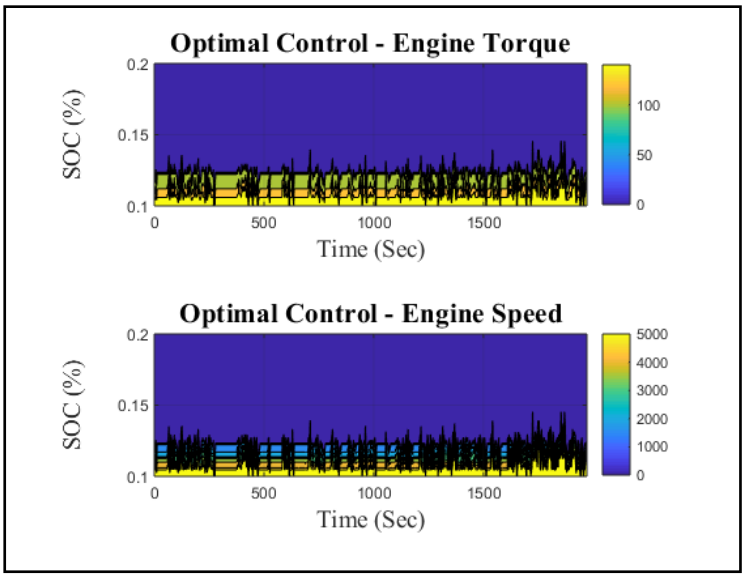

Figure 30. The Optimal Control Matrix Obtained by Constant Velocity Prediction with City-Highway DC

5. RESULTS

We proposed three different strategies for optimal EMS analysis, namely (1) perfect full DC prediction using dynamic programming, (2) 10-second prediction horizon MPC, and (3) 10-second horizon constant velocity prediction. To derive the globally optimal FE, DP needs full DC future prediction as an input. On the other hand, MPC only needs desired horizon future speed prediction as an input to derive optimal FE improvement. To cope with a limited perception system, constant velocity prediction only needs a desired time-step velocity prediction, and we can consider that velocity will be constant throughout the horizon. These three cases are simulated and presented in a separate figure. Figure 32 to Figure 41 shows each of these three Optimal EMS cases is presented next with both the highway dataset and the city-highway dataset.

5.1 Perfect Full Drive Cycle Prediction Using Dynamic Programming

Perfect full DC prediction implemented with dynamic programming provides maximum possible FE improvement over baseline FE. This is a critical data point because it can act as a benchmark for other optimal EMS for comparison. We simulated three of each perfect full highway DC and full city-highway DC prediction with DP and presented each of FE improvement over baseline FE along with the average FE improvement in Table 1 and Table 2 Also, Figure 31 and Figure 32 shows the engine power, fuel consumption and SOC comparison of full DC prediction using DP with baseline (All plots represent simulation results of DC1).

Table 1. DP Optimal FE Improvement Over Baseline with Highway DC.

DP: Fuel Economy Improvement Over Baseline			
	MPGe (%)	**1st SOC (%)**	**Last SOC (%)**
DC1	2.96	13.64	13.62
DC2	2.89	13.64	13.63
DC3	2.96	13.64	13.63
Average	2.94		

Table 1 and Table 2 shows global FE improvement over baseline FE for highway DC and city-highway DC, and the average FE improvement across all drive cycles is 2.94%, 4.32%, respectively. Also, for both the DCs the initial SOC and final SOC calculations show, we successfully achieved charge sustaining mode with highway and city-highway data set.

Table 2. DP Optimal FE Improvement Over Baseline with City-Highway DC.

DP: Fuel Economy Improvement Over Baseline			
	MPGe (%)	**1st SOC (%)**	**Last SOC (%)**
DC1	4.51	13.64	13.64
DC2	4.59	13.64	13.63
DC3	3.86	13.64	13.63
Average	4.32		

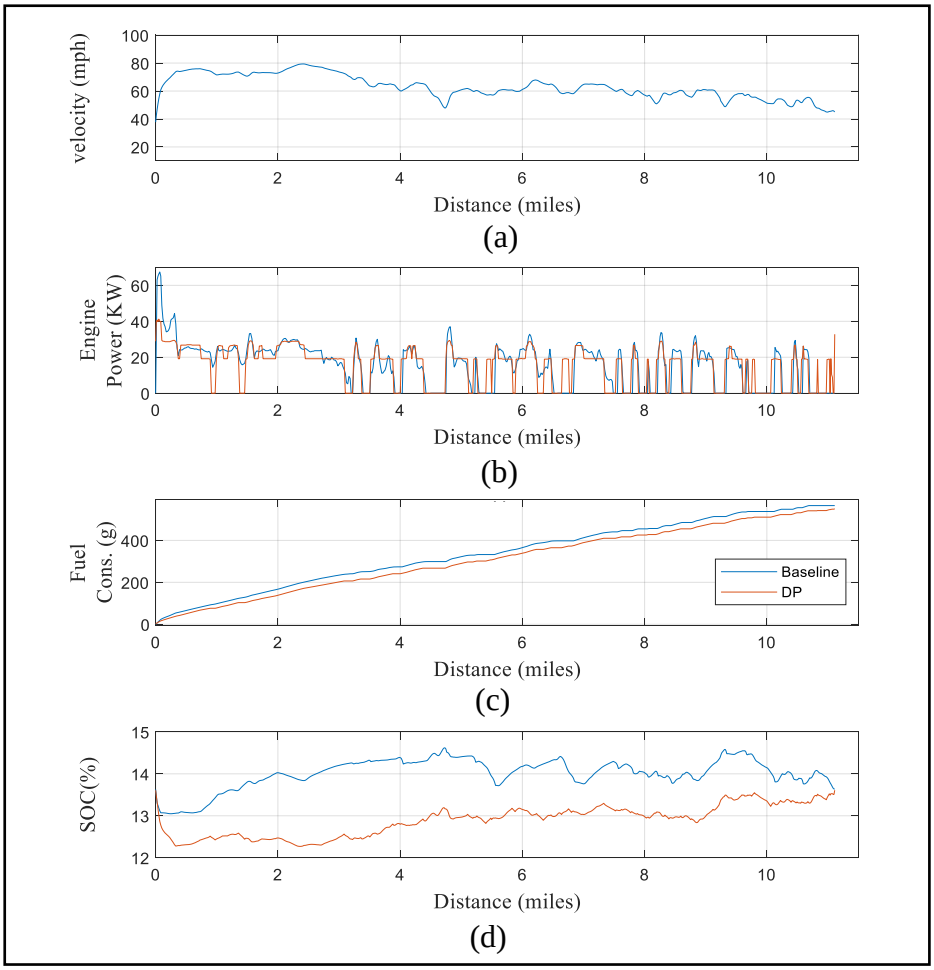

Figure 31. Baseline EMS Vs. Optimal EMS with Dynamic Programming on Highway DC

Figure 31 (a-d) and Figure 32 (a-d) shows the velocity profile, engine power, fuel consumption, and SOC over time of full highway DC, and full city-highway DC prediction using DP with baseline performance. When comparing the engine power from the Baseline EMS and the globally Optimal EMS in Figure 31 (b), there are few points like at 4th, 12th mile distance, where the Optimal EMS has turned off the engine and operated the engine at lower overall power with fewer fluctuations resulting in the FE improvement. Similarly, when comparing the engine power from the Baseline EMS and the globally Optimal EMS in Figure 32 (b), there are many points where the Optimal EMS has turned off the engine and operated the engine at lower overall power with fewer fluctuations resulting in the FE improvement. Both highway and city-highway DC's fuel consumption tends also reflects the same with less cumulative fuel consumed by optimal EMS.

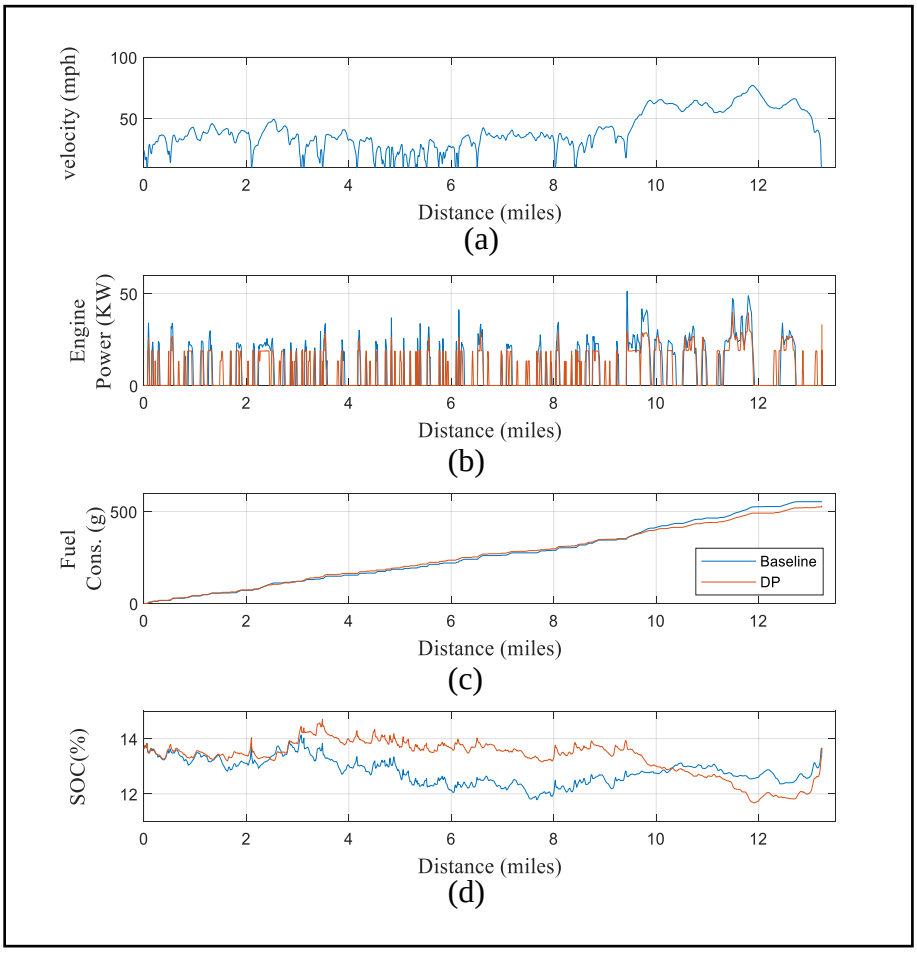

Figure 32. Baseline EMS Vs. Optimal EMS with Dynamic Programming on City-Highway DC

5.2 10-Second Prediction Horizon With MPC

The DP with perfect full DC prediction is difficult to implement in real vehicles due to its high computational cost and complexity. However, the recent advancement in driver assistance technologies taps the potential of the perception system to improve vehicular FE on a future time horizon shorter than the whole DC. This is an advantageous data point, as it provides maximum and real-world implementable optimal FE with an advance perception system. Here also we simulated 3 of each highway DC and city-highway DC with 10-second prediction horizon using MPC and presented each of FE improvement over baseline FE along with the average FE improvement in Table 3 and Table 4. Also, Figure 33 and Figure 34 show the engine power, fuel consumption, and SOC comparison of the 10-second prediction horizon using MPC with baseline (All plots represent simulation results of DC1).

Table 3. MPC Optimal FE Improvement Over Baseline with Highway DC.

MPC: Fuel Economy Improvement Over Baseline			
	MPGe (%)	**1st SOC (%)**	**Last SOC (%)**
DC1	1.87	13.64	13.63
DC2	1.84	13.64	13.63
DC3	1.84	13.64	13.64
Average	1.85		

Table 4. MPC Optimal FE Improvement Over Baseline with City-Highway DC.

MPC: Fuel Economy Improvement Over Baseline			
	MPGe (%)	**1st SOC (%)**	**Last SOC (%)**
DC1	3.32	13.64	13.63
DC2	2.95	13.64	13.63
DC3	2.61	13.64	13.66
Average	2.96		

Table 3 and Table 4 shows FE improvement over baseline FE for highway DC and city-highway DC, and the average FE improvement across all drive cycles is 1.85%, 2.96%

respectively. Also, both the DC's the initial SOC and final SOC calculations shows, we successfully achieved charge sustaining mode with highway and city-highway data set.

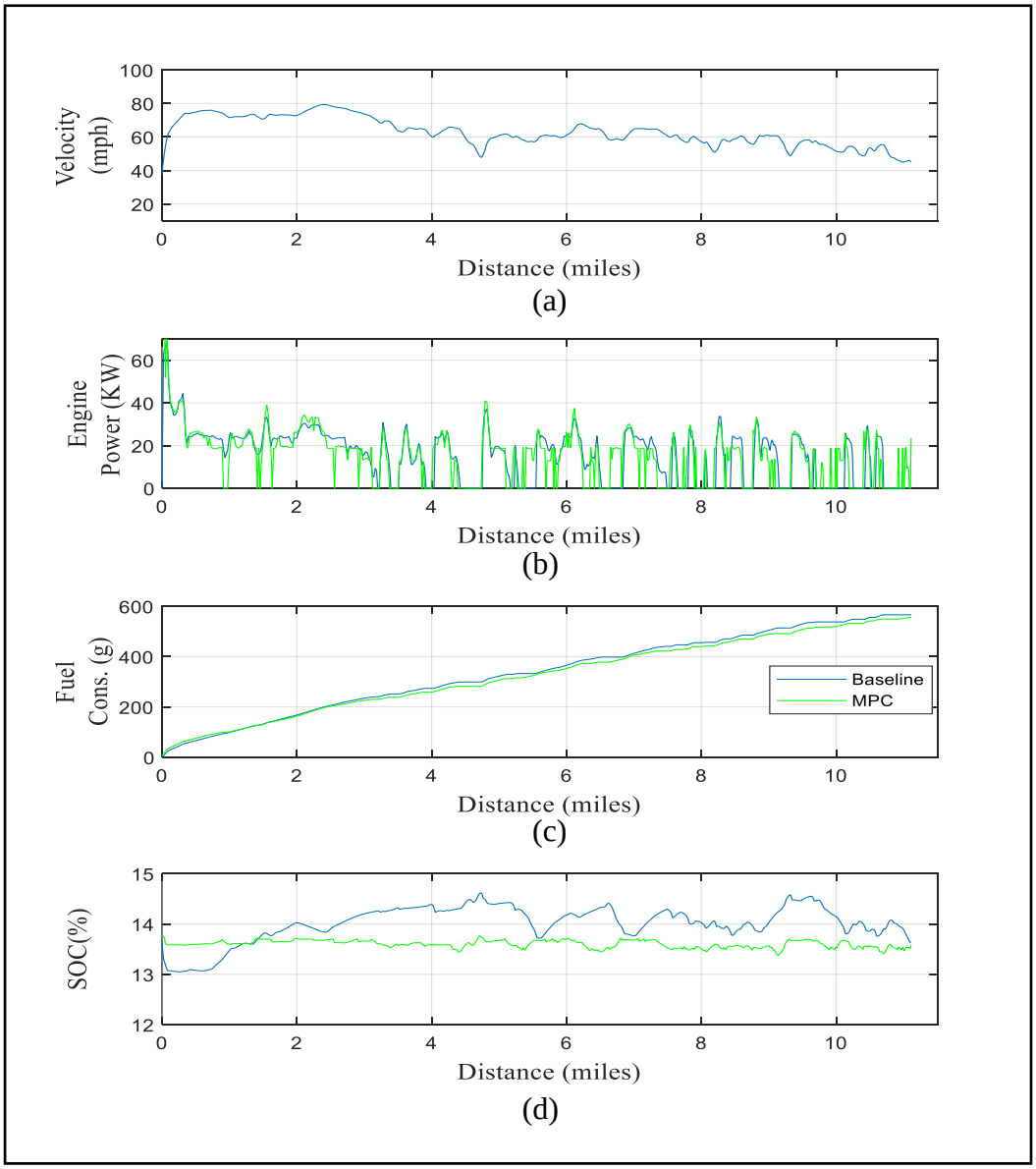

Figure 33. Baseline EMS Vs. Optimal EMS with MPC on Highway DC

Figure 33 (a-d) and Figure 34 (a-d) shows the velocity profile, engine power, fuel consumption, and SOC of 10-second horizon highway and city-highway DC's prediction using MPC with baseline performance respectively. When comparing the engine power from the Baseline EMS and the 10-second horizon with MPC Optimal EMS in Figure 33 (b), the Optimal EMS tends to operate the engine at lower power and a more consistent power

resulting in the FE savings. Similarly, when comparing the engine power from the Baseline EMS and the 10-second horizon with MPC Optimal EMS in Figure 34 (b), Optimal EMS yields similar lower engine power as with the highway DC, which resulting in an FE increase. Both highway and city-highway DC's fuel consumption tends also reflects the same with less cumulative fuel consumed by optimal EMS.

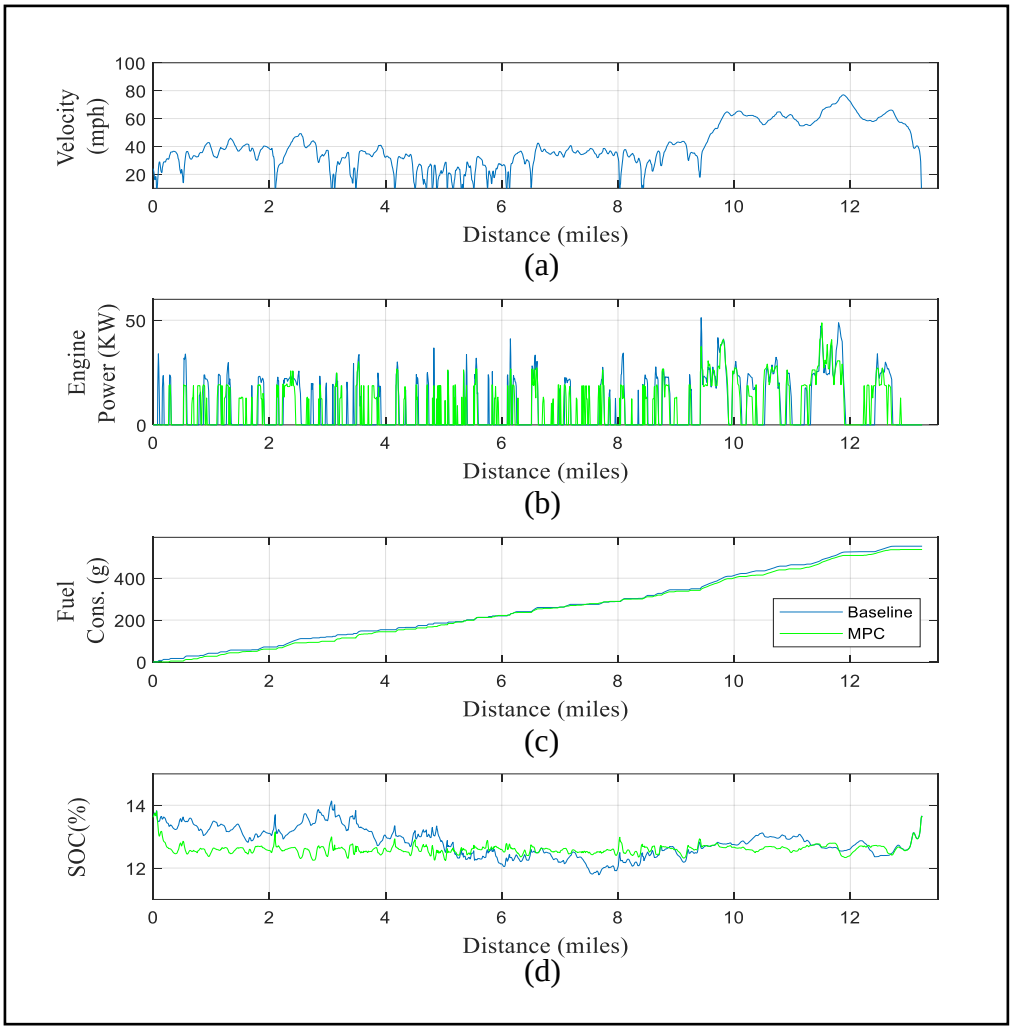

Figure 34. Baseline EMS Vs. Optimal EMS with MPC on City-Highway DC

5.3 10-Second Prediction Horizon with Constant Velocity Prediction

MPC has advantages like very significant and real-world implementable optimal FE over the finite horizon with an advanced perception system. Even though it requires a very advance perception system; however, in the current state, there is a need to develop a control strategy that can work with limited perception and provides some FE improvement over

baseline FE. So, we have developed a control strategy which can provide significant FE improvement with limited perception of future vehicle operation. Here also, we simulated 3 of each highway DC and city-highway DC with a 10-second prediction horizon using constant velocity prediction where velocity is assumed constant for the entire horizon and presented each of FE improvement over baseline FE along with the average FE improvement in Table 5 and Table 6. Also, Figure 35 and Figure 36 show the engine power, fuel consumption, and SOC comparison of 10-second prediction horizon using constant velocity prediction with baseline (All plots represent simulation results of DC1).

Table 5. Constant Velocity Prediction Optimal FE Improvement Over Baseline with Highway DC.

Constant Velocity: Fuel Economy Improvement Over Baseline			
	MPGe (%)	**1st SOC (%)**	**Last SOC (%)**
DC1	1.71	13.64	13.62
DC2	1.47	13.64	13.63
DC3	1.58	13.64	13.63
Average	1.58		

Table 5 and Table 6 shows non-global FE improvement over baseline FE for highway and city-highway DC's, and the average FE improvement across all drive cycles is 1.58%, 2.45%, respectively. Also, both DC's the initial SOC, and final SOC calculations show, we successfully achieved charge sustaining mode with highway and city-highway data set.

Table 6. Constant Velocity Prediction Optimal FE Improvement Over Baseline with City-Highway DC.

Constant Velocity: Fuel Economy Improvement Over Baseline			
	MPGe (%)	**1st SOC (%)**	**Last SOC (%)**
DC1	2.45	13.64	13.63
DC2	2.51	13.64	13.66
DC3	2.41	13.64	13.64
Average	2.45		

Figure 35 (a-d) and Figure 36 (a-d) shows the velocity profile, engine power, fuel consumption, and SOC of a full highway and city-highway DC's prediction using 10-Second Constant Velocity Prediction with baseline performance. When comparing the engine power from the Baseline EMS and the non-globally Optimal EMS in Figure 35 (b), there are very few points where the Optimal EMS has turned off the engine and operated the engine at lower overall power with fewer fluctuations resulting in the FE improvement. Similarly, when comparing the engine power from the Baseline EMS and the globally Optimal EMS in Figure 36 (b), Optimal EMS yields similar lower engine power as with the highway DC, which resulting in an FE increase. Both highway and city-highway DC's fuel consumption tends also reflects the same with less cumulative fuel consumed by optimal EMS.

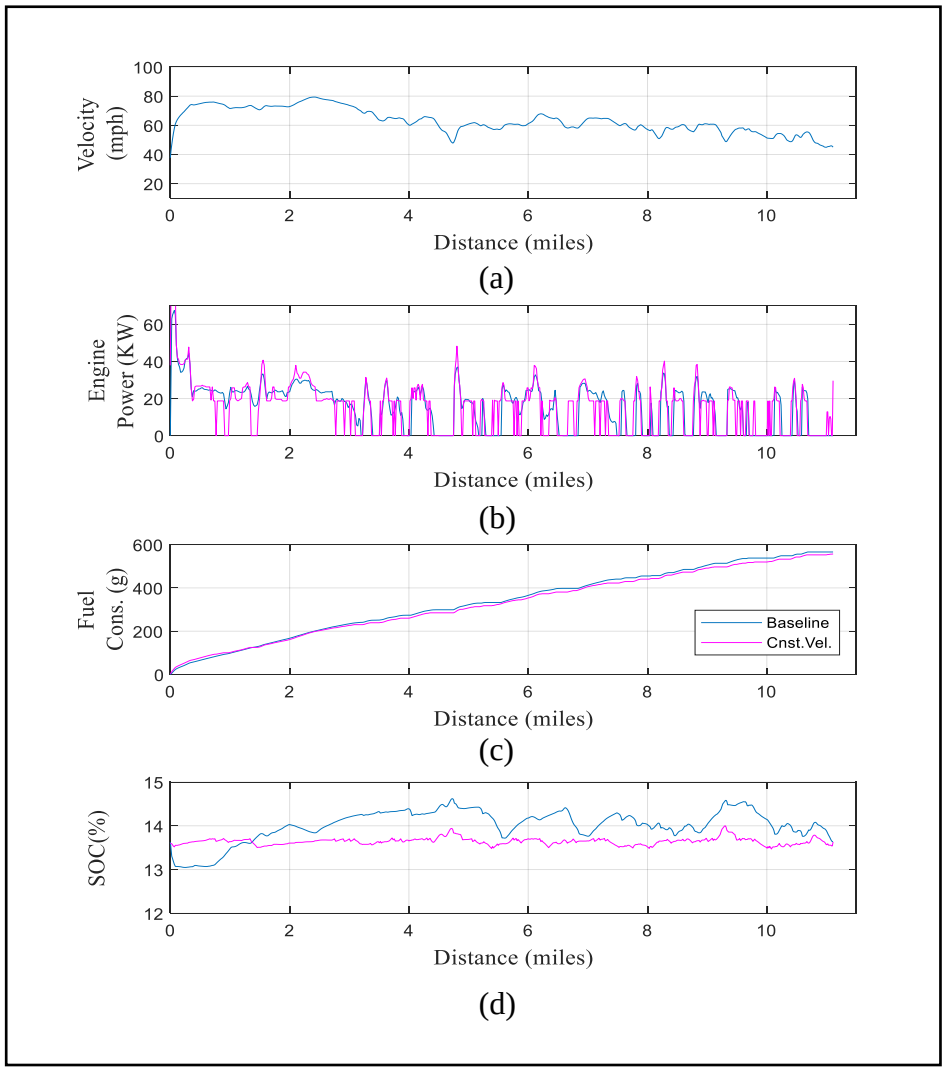

Figure 35. Baseline EMS Vs. Optimal EMS with Constant Velocity Prediction on Highway DC

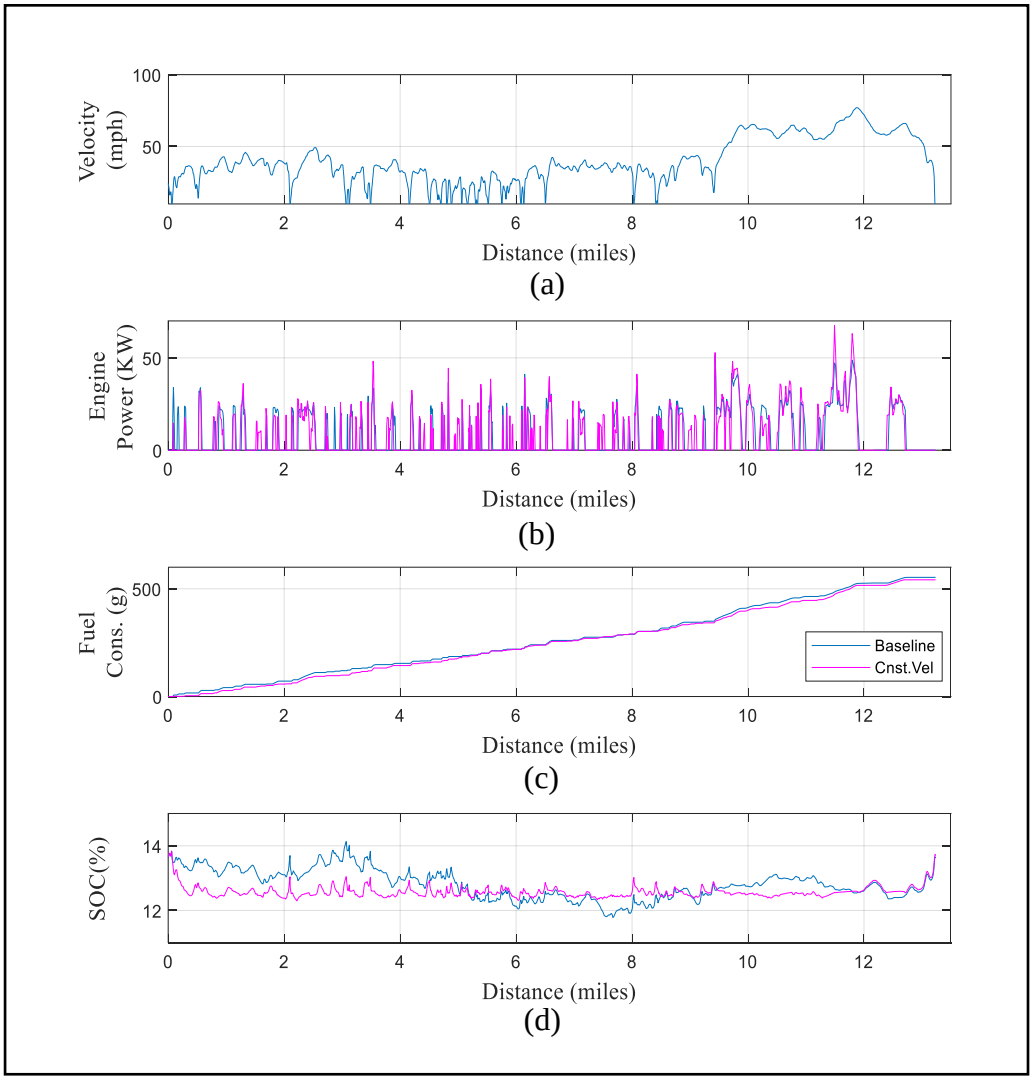

Figure 36. Baseline EMS Vs. Optimal EMS with Constant Velocity Prediction on City-Highway DC

5.4 Combined Results: Fuel Consumption and SOC

Figure 38 and Figure 39 compares the result of fuel consumption and SOC level with highway DC and city-highway DC respectively at each time index of all three strategies with baseline EMS which outlines the current performance of a vehicle in a rules-based, non-predictive control strategy.

Table 7 and 8 shows the average FE improvement and Figure 38-39 (a), 38-39 (b) and 38-39 (c) shows the overall fuel consumption trend (DC1 plots) from lowest to highest can be given as:

DP < MPC < Constant Velocity Prediction < Baseline EMS

Perfect full DC prediction implemented with DP shows the best FE improvement and is considered as the upper limit on FE improvement. On the contrary, the baseline EMS shows the point of comparison for any FE improvement

Figure 37 (b) shows a constant velocity prediction fuel consumption trend closely follows the MPC on highway driving; on the contrary, Figure 38 (b) shows a significant difference between constant velocity prediction and MPC fuel consumption trends. However, it shows that even with the limited prediction, constant velocity prediction strategy can provide remarkable FE improvement. Also, all EMS strategies start and end with the same SOC level, which verifies that "charge sustaining" mode is being enforced.

Table 7. Average DP, MPC, and Constant Velocity Prediction Optimal FE Improvement Over Baseline with Highway DC.

Fuel Economy Improvement Over Baseline			
	MPGe (%)	**1st SOC (%)**	**Last SOC (%)**
DP	2.94	13.64	13.64
MPC	1.85	13.64	13.62
Constant Velocity	1.58	13.64	13.62

Table 8. Average DP, MPC, and Constant Velocity Prediction Optimal FE Improvement Over Baseline with City-Highway DC.

Fuel Economy Improvement Over Baseline			
	MPGe (%)	**1st SOC (%)**	**Last SOC (%)**
DP	4.32	13.63	13.64
MPC	2.96	13.63	13.62
Constant Velocity	2.45	13.63	13.62

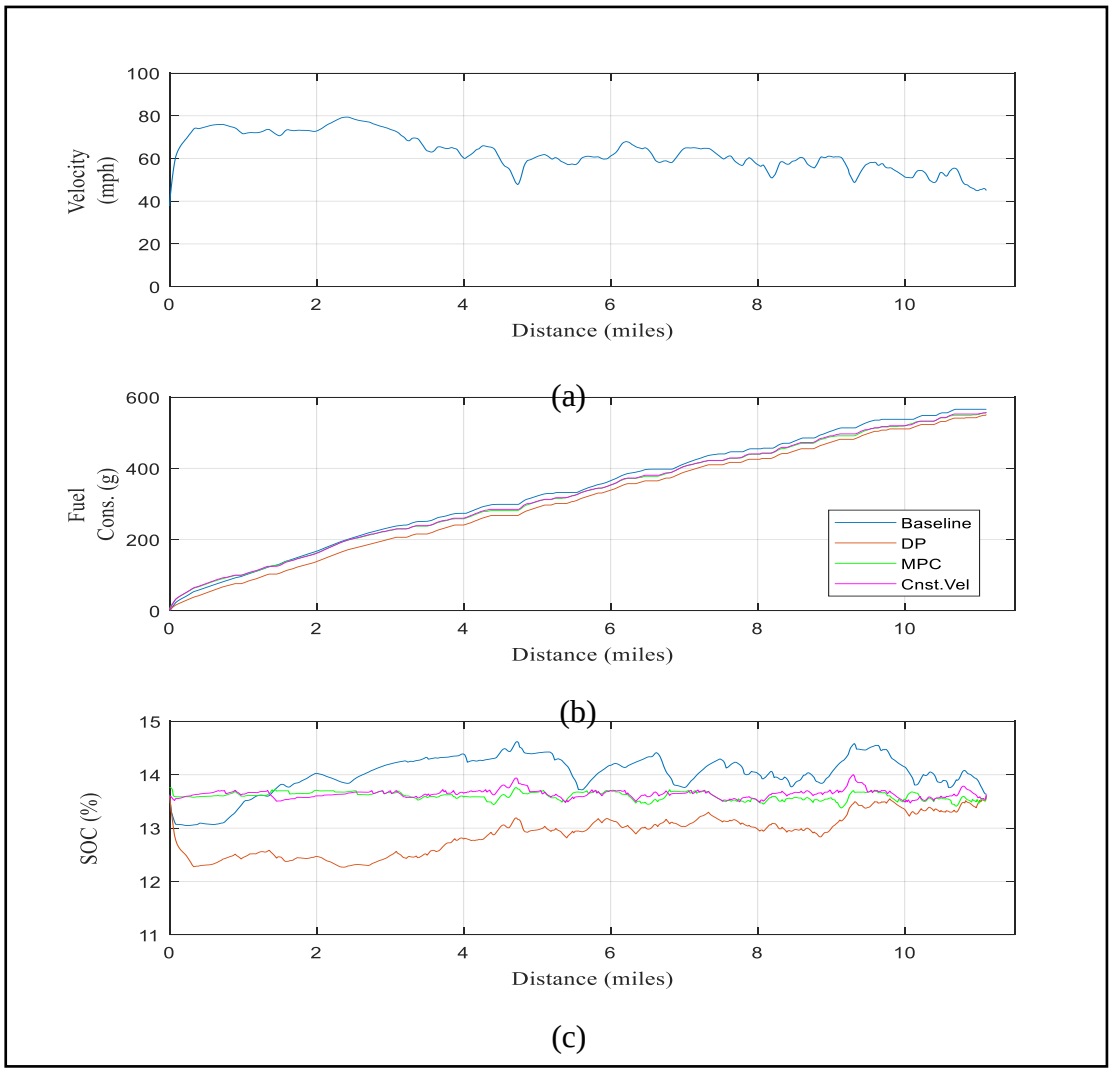

Figure 37. Baseline, DP, MPC, and Constant Velocity Prediction EMS Comparisons with Highway DC

From Figure 37 - 38 (c), SOC trends of DP strictly obey charge sustaining operation, but in between the DC endpoints, SOC fluctuates broadly. This clearly indicates that DP takes full advantage of battery power with perfect full DC prediction. Due to this in both highway and city-highway driving, FE improvement is biggest. This is also justified by the DP fuel consumption trends shown in Figure 37 – 38 (b). This clearly shows that the low DP fuel consumption trend is distinct from others.

Figure 37 (c) indicates that on highway driving, SOC trends of both MPC and constant velocity prediction at each time-step always stay close to the initial SOC level, which looks like the SOC level is constant for whole DC. This indicates that due to

application of DP only for finite horizon, it restricts the MPC from taking advantage of battery SOC, and it tries to maintain chare sustaining mode. On the other hand, with city-highway driving, the SOC trends of both MPC and constant velocity prediction shows some fluctuations, but their amplitude is much smaller than the DP SOC trend. This low SOC fluctuation results in higher battery life.

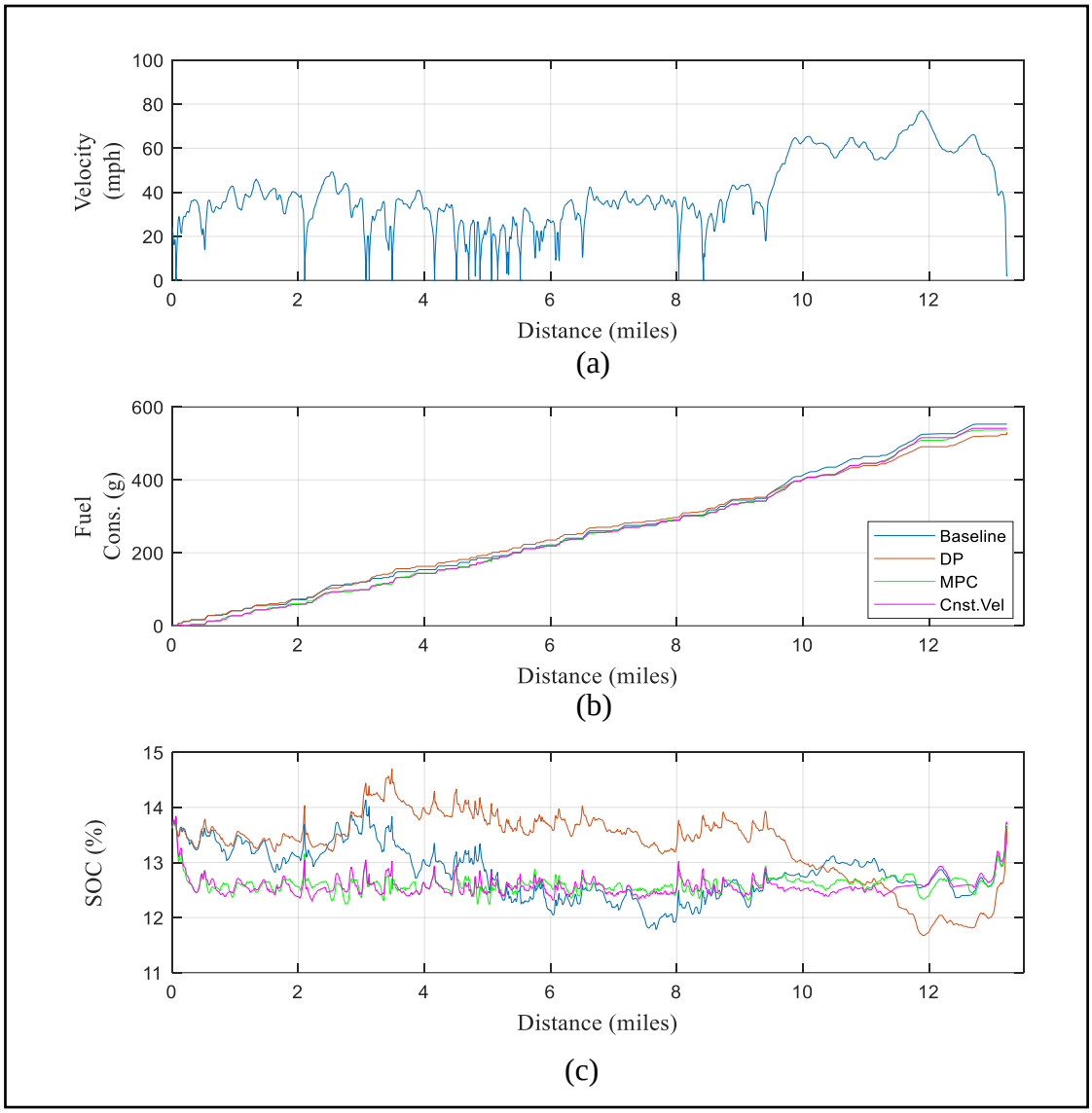

Figure 38. Baseline, DP, MPC, and Constant Velocity Prediction EMS Comparisons with City-Highway DC

6. Combined Results: Engine Power

Figure 39 and Figure 40 compare engine power trends of different EMS strategies on

the highway and city-highway driving, respectively. From Figure 39 – 40 (a), the engine power comparison of DP with baseline performance shows relatively lower overall power resulting in 2.94% and 4.3% of average FE improvement over baseline fuel consumption for highway and city-highway driving, respectively.

Figure 39 – 40 (b) shows that the MPC engine power trend closely follows the DP engine power trend with some exceptions. MPC has the potential to achieve 60% - 65% and 70% - 80% of global FE improvement levels on the highway and city-highway DC, respectively.

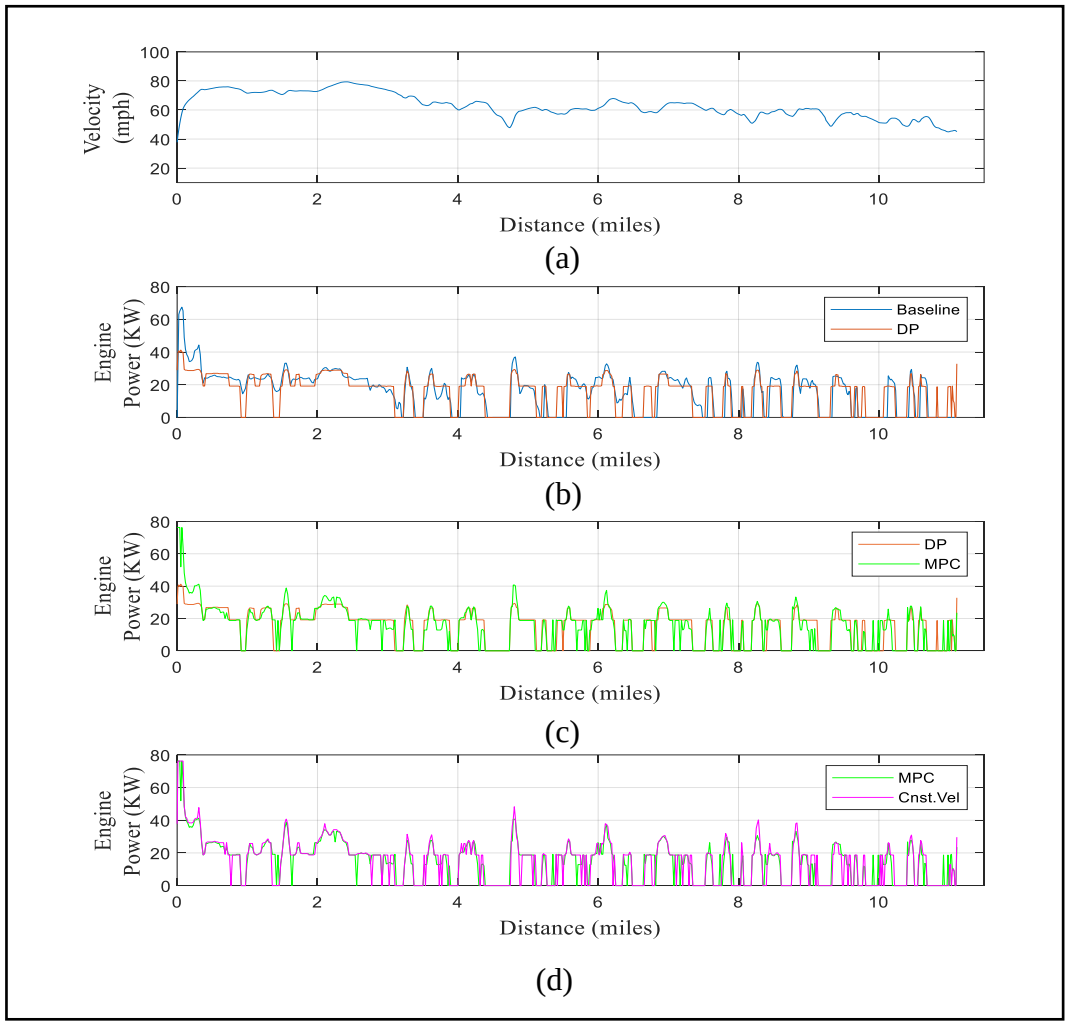

Figure 39. Baseline, DP, MPC, and Constant Velocity Prediction Engine Power Comparisons with Highway DC.

Figure 39 (c) indicates on highway DC in some instances; there is a sharp increment in the engine power for the constant velocity prediction as compared to MPC engine power.

This indicates that constant velocity prediction can potentially achieve 80% - 92% of MPC FE improvement. On the other hand, the engine power trend with constant velocity prediction shows multiple sharp increments over MPC engine power on city-highway DC, as shown in Figure 40 (c). This causes the drop in FE improvement potential of constant velocity prediction over MPC FE improvement. Overall the constant velocity prediction has the potential to achieve 50% - 60% of global FE improvement.

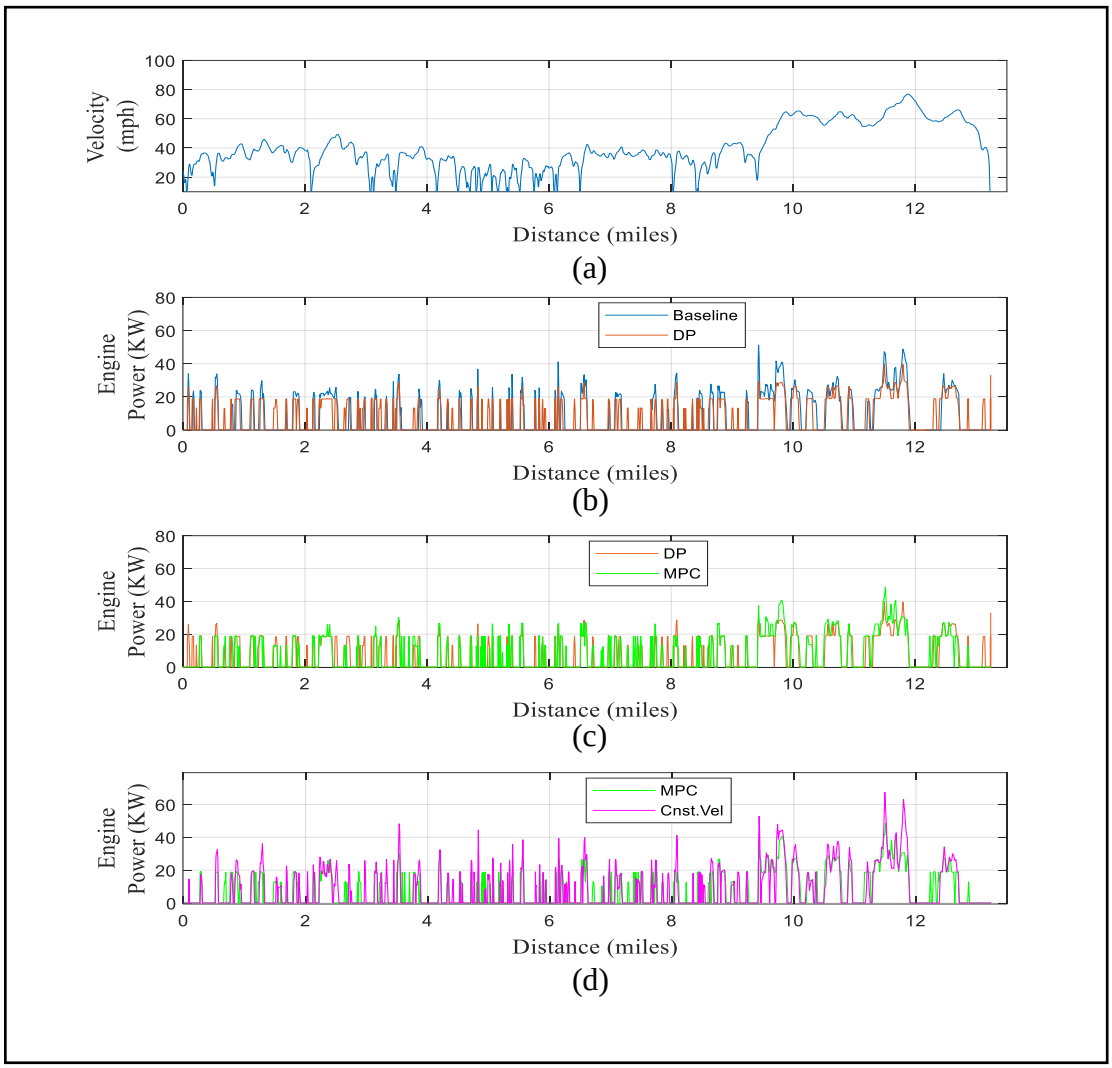

Figure 40. Baseline, DP, MPC, and Constant Velocity Prediction Engine Power Comparisons with City-Highway DC.

6. SUMMARY

Overall the FE improvement results of both highway and city-highway driving with all 3 strategies over baseline EMS are shown in Figure 41 and Table 9. The perfect full DC prediction along with DP has the largest average FE improvement, followed by 10-second prediction horizon MPC, and then 10-second horizon constant velocity prediction over baseline EMS.

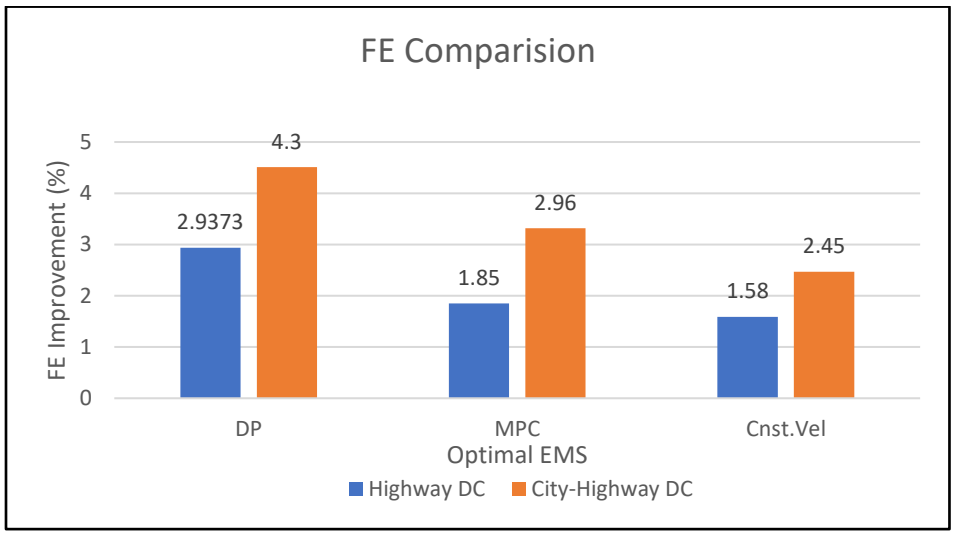

Figure 41. Overall Average FE Improvement Over Baseline with All 3 EMS with Both Highway and City-Highway DC

Table 9. Overall Average FE Improvement Over Baseline with All 3 EMS with Both Highway and City-Highway DC.

Average Fuel Economy Improvement Over Baseline (%)		
	Highway DC	**City-Highway DC**
DP	2.94	4.3
MPC	1.85	2.96
Constant Velocity	1.58	2.45

Figure 41 also indicates that on the highway DC constant velocity prediction can achieve nearly equal FE improvement of MPC FE improvement. So, on highway driving, it could be better to use the more straightforward constant velocity prediction method than the complicated MPC method as constant velocity prediction does not require perfect horizon prediction like MPC. On the contrary, with city-highway DC, the gap between MPC and constant velocity prediction FE improvement is significant. This means with city-highway DC, MPC gives better results because it considers perfect horizon velocity predictions.

7. CONCLUSION

In this study, I have investigated 3 different energy management strategies in simulation using real-world highway and city-highway DC in a validated, control-oriented 2017 Toyota Prius Prime model operating in charge sustaining mode. The input to all the EMS planning sub-system is velocity predictions obtained from the perception sub-system. The output of the given planning sub-system is the vehicle control matrix which realizes FE improvement with optimal engine power generation while maintaining charge sustention mode.

The perfect full DC prediction along with DP gives globally optimal EMS which represents the upper limit on achievable FE improvement. The 10-second prediction window MPC strategy provides the second-best FE improvement results in my research which were found to be very significant. The MPC results suggest that, it has potential to achieve 60%-65% and 70% - 80% of global FE improvement over highway and city-highway DC respectively. So, with the advancement in perception systems, MPC can be implemented in real vehicles. Whereas, the constant velocity prediction results also show prospects of implementation in vehicle controllers with MPC type of framework. The constant velocity prediction results suggest that has the potential to achieve 80%-90% and 75% - 85% of MPC FE improvement over highway and city-highway DC respectively. Also, the MPC and constant velocity prediction results suggest that FE improvement from perfect 10 second MPC is only slightly higher than constant velocity 10 second. This means that a 10 second prediction window is not that beneficial for generating actual velocity predictions for MPC. The MPC and Constant velocity SOC results corroborate the above claim(s) to achieve better battery performance.

8. FUTURE STUDY

For future work, we seek to combine both perception and planning sub-system and integrate it with a real-world vehicle through NVIDIA PX2 and vehicle controller. Along with fuel economy, our goal is to combine the vehicular emissions model with a neural network to accomplish the ultimate goal of efficient vehicle powertrain. Our near-term goal is to implement the constant velocity prediction strategy as it does not require perfect horizon operation prediction. As the 10 second prediction window is not that beneficial for generating actual velocity predictions for MPC, we seek to explore more prediction windows, and its effect on FE improvement. Our long-term goal is to implement the model predictive control strategy as our perception research gets mature.

REFERENCES

[1] International Energy Agency, “Key World Energy Statistics 2016,” International Energy Agency, 2015.

[2] U.S Department of Energy (2016) NEXT-Generation Energy Technologies for Connected and Automated on-Road-vehicles (NEXTCAR) Program Overview.

[3] International Energy Agency (2015) Energy and Climate Change - World Energy Outlook Special Report.

[4] Thrun S (2010) Toward robotic cars. Commun ACM 53:99–106.

[5] Zulkefli, M.A.M., Zheng, J., Sun, Z., and Liu, H.X., “Hybrid Powertrain Optimization with Trajectory Prediction Based on Inter-Vehicle-Communication and VehicleInfrastructure-Integration,” Transportation Research Part C: Emerging Technologies 45:41-63, 2014.

[6] Asher, Z., Patil, A., Wifvat, V., Frank, A. et al., "Identification and Review of the Research Gaps Preventing a Realization of Optimal Energy Management Strategies in Vehicles," SAE Int. J. Alt. Power. 8(2):2019.

[7] Tunnell, Jordan, Zachary D. Asher, Sudeep Pasricha, and Thomas H. Bradley. "Toward improving vehicle fuel economy with ADAS." SAE International Journal of Connected and Automated Vehicles 1, no. 12-01-02-0005 (2018): 81-92.

[8] Baker, David, Zachary D. Asher, and Thomas Bradley. V2V communication based real-world velocity predictions for improved HEV fuel economy. No. 2018-01-1000. SAE Technical Paper, 2018.

[9] Zhang P, Yan F, Du C (2015/8) A comprehensive analysis of energy management strategies for hybrid electric vehicles based on bibliometrics. Renewable Sustainable Energy Rev 48:88–104

[10] Onori, Simona, Lorenzo Serrao, and Giorgio Rizzoni. Hybrid electric vehicles: energy management strategies. Vol. 13. Berlin Heidelberg: Springer, 2016.

[11] Wu, Guoyuan, Xuewei Qi, Matthew Barth, and Kanok Boriboonsomsin. "Advanced Energy Management Strategy Development for Plug-in Hybrid Electric Vehicles." (2016).

[12] Asher, Zachary D., Van Wifvat, Anthony Navarro, Scott Samuelsen, and Thomas Bradley. The importance of HEV fuel economy and two research gaps preventing real world implementation of optimal energy management. No. 2017-26-0106. SAE Technical Paper, 2017.

[13] Onori, Simona, Lorenzo Serrao, and Giorgio Rizzoni. "Adaptive equivalent consumption minimization strategy for hybrid electric vehicles." In ASME 2010 dynamic systems and control conference, pp. 499-505. American Society of Mechanical Engineers Digital Collection, 2011. J. Wang, “Fundamentals of erbium-doped fiber amplifiers arrays (Periodical style—Submitted for publication),” IEEE J. Quantum Electron., submitted for publication.

[14] Borhan, H. Ali, Ardalan Vahidi, Anthony M. Phillips, Ming L. Kuang, and Ilya V. Kolmanovsky. "Predictive energy management of a power-split hybrid electric vehicle." In 2009 American control conference, pp. 3970-3976. IEEE, 2009.

[15] Asher, Zachary D., David A. Baker, and Thomas H. Bradley. "Prediction error applied to hybrid electric vehicle optimal fuel economy." IEEE Transactions on Control Systems Technology 26, no. 6 (2017): 2121-2134.

[16] Rajamani, Rajesh. Vehicle dynamics and control. Springer Science & Business Media, 2011.

[17] Gong Q, Li Y, Peng Z (2009) Power management of plug-in hybrid electric vehicles using neural network based trip modeling. In: 2009 American Control Conference. ieeexplore.ieee.org, pp 4601–4606

[18] Bender FA, Kaszynski M, Sawodny O (2013) Drive Cycle Prediction and Energy Management Optimization for Hybrid Hydraulic Vehicles. IEEE Trans Veh Technol 62:3581–3592

[19] Mohd Zulkefli MA, Zheng J, Sun Z, Liu HX (2014/8) Hybrid powertrain optimization with trajectory prediction based on inter-vehicle-communication and vehicle-infrastructure-integration. Transp Res Part C: Emerg Technol 45:41–63

[20] Sun, Chao, Xiaosong Hu, Scott J. Moura, and Fengchun Sun. "Velocity predictors for predictive energy management in hybrid electric vehicles." IEEE Transactions on Control Systems Technology 23, no. 3 (2014): 1197-1204.

[21] Baker D, Asher Z, Bradley T (2017) Investigation of Vehicle Speed Prediction from Neural Network Fit of Real-World Driving Data for Improved Engine On/Off Control of the EcoCAR3 Hybrid Camaro. SAE Technical Paper

[22] Asher, Zachary D., Jordan A. Tunnell, David A. Baker, Robert J. Fitzgerald, Farnoush Banaei-Kashani, Sudeep Pasricha, and Thomas H. Bradley. Enabling Prediction for Optimal Fuel Economy Vehicle Control. No. 2018-01-1015. SAE Technical Paper, 2018.

[23] Liu, Kuan, Zachary Asher, Xun Gong, Mike Huang, and Ilya Kolmanovsky. Vehicle Velocity Prediction and Energy Management Strategy Part 1: Deterministic and Stochastic Vehicle Velocity Prediction Using Machine Learning. No. 2019-01-1051. SAE Technical Paper, 2019.

[24] Gaikwad, Tushar D., Zachary D. Asher, Kuan Liu, Mike Huang, and Ilya Kolmanovsky. Vehicle Velocity Prediction and Energy Management Strategy Part 2: Integration of Machine Learning Vehicle Velocity Prediction with Optimal Energy Management to Improve Fuel Economy. No. 2019-01-1212. SAE Technical Paper, 2019.

[25] Qi X, Luo Y, Wu G, Boriboonsomsin K, Barth M (2019) Deep reinforcement learning enabled self-learning control for energy efficient driving. Transp Res Part C: Emerg Technol 99:67–81

[26] Del Re, Luigi, Frank Allgöwer, Luigi Glielmo, Carlos Guardiola, and Ilya Kolmanovsky, eds. Automotive model predictive control: models, methods and applications. Vol. 402. Springer, 2010.

[27] Jeong, Jongryeol, Namdoo Kim, Kevin Stutenberg, and Aymeric Rousseau. Analysis and Model Validation of the Toyota Prius Prime. No. 2019-01-0369. SAE Technical Paper, 2019.

[28] Moura, Scott Jason, Hosam K. Fathy, Duncan S. Callaway, and Jeffrey L. Stein. "A stochastic optimal control approach for power management in plug-in hybrid electric vehicles." IEEE Transactions on control systems technology 19, no. 3 (2010): 545-555.

[29] Asher, Zachary D., David A. Trinko, and Thomas H. Bradley. "Increasing the fuel economy of connected and autonomous lithium-ion electrified vehicles." In Behaviour of Lithium-Ion Batteries in Electric Vehicles, pp. 129-151. Springer, Cham, 2018.

[30] Asher, Zachary D., Abril A. Galang, Will Briggs, Brian Johnston, Thomas H. Bradley, and Shantanu Jathar. Economic and Efficient Hybrid Vehicle Fuel Economy and Emissions Modeling Using an Artificial Neural Network. No. 2018-01-0315. SAE Technical Paper, 2018.

[31] Kirk, Donald E. Optimal control theory: an introduction. Courier Corporation, 2012.

[32] Gong, Qiuming, Yaoyu Li, and Zhong-Ren Peng. "Trip-based optimal power management of plug-in hybrid electric vehicles." IEEE Transactions on vehicular technology 57, no. 6 (2008): 3393-3401.

[33] Xie, Shaobo, Xiaosong Hu, Zongke Xin, and James Brighton. "Pontryagin's minimum principle-based model predictive control of energy management for a plug-in hybrid electric bus." Applied energy 236 (2019): 893-905.

[34] Borhan, Hoseinali, Ardalan Vahidi, Anthony M. Phillips, Ming L. Kuang, Ilya V. Kolmanovsky, and Stefano Di Cairano. "MPC-based energy management of a power-split hybrid electric vehicle." IEEE Transactions on Control Systems Technology 20, no. 3 (2011): 593-603.

[35] Fu, Lina, Ö. Ümit, Pinak Tulpule, and Vincenzo Marano. "Real-time energy management and sensitivity study for hybrid electric vehicles." In Proceedings of the 2011 American Control Conference, pp. 2113-2118. IEEE, 2011.

[36] Huang, Mike, Zhang, Shengqi, and Yushi Shibaike " Real time Long Horizon Model Predictive Control of a Plug in Hybrid Vehicle Power Split Utilizing Trip Preview." JSAE 20199015 (2019)

[37] Meyer, Richard, Raymond A. DeCarlo, Peter H. Meckl, Chris Doktorcik, and Steve Pekarek. "Hybrid model predictive power flow control of a fuel cell-battery vehicle." In Proceedings of the 2011 American Control Conference, pp. 2725-2731. IEEE, 2011.

[38] Meyer, Richard T., Raymond A. DeCarlo, Peter H. Meckl, Chris Doktorcik, and Steve Pekarek. "Hybrid model predictive power management of a fuel cell-battery vehicle." Asian Journal of Control 15, no. 2 (2013): 363-379.

[39] Meyer, Richard T., Raymond A. DeCarlo, and Steve Pekarek. "Hybrid Model Predictive Power Management of a Battery-Supercapacitor Electric Vehicle." Asian Journal of Control 18, no. 1 (2016): 150-165.

APPENDIX

Let's start with state of charge dynamics [14, 15],

$$SOC(k+1) = SOC(k) - \left\{\frac{V_{OC} - \sqrt{{V_{OC}}^2 - (4 \times P_{Batt} \times R_{Batt})}}{2 \times R_{Batt} \times Q_{Batt\_0}}\right\} \ldots\ldots\ldots\ldots\ldots\ldots\ldots\ldots\text{I}$$

Where,

$SOC(k+1)$ = State of charge of next state

$SOC(k)$ = State of charge of current state

V_{OC} = Open Circuit Voltage

R_{Batt} = Battery Resistance

Q_{Batt} = total/maximum charge of fully charged battery

P_{Batt} = Battery Power

Let, Power discharge from the battery to the motor and charging from the generator to the battery is given by [14, 15],

$P_{Batt} = P_G + P_M$

Where,

P_G = Generator Power.

P_M = Motor Power.

Now find $P_G, and P_M$

generator and motor power are calculated using torque and speed of generator and motor respectively as follows [14, 15],

$P_G = [\eta^k \times \tau_G \times \omega_G]$

$$P_G = \eta^k \times \left(\tau_{ICE} \times \left(\frac{\rho}{1+\rho}\right)\right) \times \left(\left(\omega_{ICE} \times \left(\frac{1+\rho}{\rho}\right)\right) - \left(\frac{V}{R_t \times r_{final} \times \rho}\right)\right)$$

$P_M = [\eta^k \times \tau_M \times \omega_M]$

$$P_M = \eta^k \times \left(\frac{V}{R_t \times r_{final} \times \rho}\right) \times \left(\left(\tau_P \times r_{final}\right) - \left(\frac{\tau_{ICE}}{1+\rho}\right)\right)$$

Where,

η = Electrochemical conversion efficiency

k = -1 during discharging and 1 during charging

τ_G = Electric Machine1 or Generator Torque.

τ_M = Electric Machine1 or Motor Torque.

ρ = Gear ratio between sun gear and the ring gear = $\frac{radius\ of\ sun\ gear\ (R_s)}{radius\ of\ ring\ gear\ (R_r)}$

R_t = Wheel/tire radius

r_{final} = Final reduction gear ratio.
V = Vehicle velocity
τ_{ICE} = Engine Torque.
ω_{ICE} = Engine Speed.
τ_P = Propulsion Torque.

Green part of equation I becomes,

$$(4 \times P_{Batt} \times R_{Batt}) = 4 \times (P_G + P_M) \times R_{Batt}$$

$$(4 \times P_{Batt} \times R_{Batt}) = 4 \times R_{Batt} \times \begin{Bmatrix} \left[\eta^k \times \left(\tau_{ICE} \times \left(\frac{\rho}{1+\rho}\right)\right) \times \left(\left(\omega_{ICE} \times \left(\frac{1+\rho}{\rho}\right)\right) - \left(\frac{V}{R_t \times r_{final} \times \rho}\right)\right)\right] + \\ \left[\eta^k \times \left(\frac{V}{R_t \times r_{final} \times \rho}\right) \times \left((\tau_P \times r_{final}) - \left(\frac{\tau_{ICE}}{1+\rho}\right)\right)\right] \end{Bmatrix}$$

Now equation 1 becomes,

$$SOC(k+1) = SOC(k) - \left(\frac{V_{OC}}{2 \times R_{Batt} \times Q_{Batt_0}}\right) + \sqrt{\left(\frac{{V_{OC}}^2}{4 \times {R_{Batt}}^2 \times {Q_{Batt_0}}^2}\right) - \left[\frac{4 \times R_{Batt} \times \eta^k \times \left(\tau_{ICE} \times \left(\frac{\rho}{1+\rho}\right)\right) \times \left(\left(\omega_{ICE} \times \left(\frac{1+\rho}{\rho}\right)\right) - \left(\frac{V}{R_t \times r_{final} \times \rho}\right)\right)}{4 \times {R_{Batt}}^2 \times {Q_{Batt_0}}^2}\right] - \left[\frac{4 \times R_{Batt} \times \eta^k \times \left(\frac{V}{R_t \times r_{final}}\right) \times \left((\tau_P \times r_{final}) - \left(\frac{\tau_{ICE}}{1+\rho}\right)\right)}{4 \times {R_{Batt}}^2 \times {Q_{Batt_0}}^2}\right]}$$

$$SOC(k+1) = SOC(k) - \left(\frac{V_{OC}}{2 \times R_{Batt} \times Q_{Batt_0}}\right) + \sqrt{\left(\frac{{V_{OC}}^2}{4 \times {R_{Batt}}^2 \times {Q_{Batt_0}}^2}\right) - \left[\frac{\eta^k \times \left(\tau_{ICE} \times \left(\frac{\rho}{1+\rho}\right)\right) \times \left(\left(\omega_{ICE} \times \left(\frac{1+\rho}{\rho}\right)\right) - \left(\frac{V}{R_t \times r_{final} \times \rho}\right)\right)}{R_{Batt} \times {Q_{Batt_0}}^2}\right] - \left[\frac{\eta^k \times \left(\frac{V}{R_t \times r_{final}}\right) \times \left((\tau_P \times r_{final}) - \left(\frac{\tau_{ICE}}{1+\rho}\right)\right)}{R_{Batt} \times {Q_{Batt_0}}^2}\right]}$$

The simplified DP equation consisting - all dynamic equations of vehicle, wheel, SOC of power-split architecture with planetary gear train arrangement is,

$$SOC(k+1) = SOC(k) - C_1 + \sqrt{C_2 - \left[C_3 \times \tau_{ICE} \times \left((C_4 \times \omega_{ICE}) - (C_5 \times V)\right)\right] - \left[C_6 \times V \times \left((C_7 \times \tau_P) - (C_8 \times \tau_{ICE})\right)\right]} \quad \text{.....II}$$

Where,

$w_1 = V =$ Vehicle velocity

$w_2 = \tau_P =$ Propulsion Torque.

$u_1 = \omega_{ICE} =$ Engine Speed.

$u_2 = \tau_{ICE} =$ Engine Torque.

$s = SOC =$ State of charge.

Equation II becomes,

$$s(k+1) = s(k) - C_1 + \sqrt{C_2 - \left[C_3 \times u_2 \times \left((C_4 \times u_1) - (C_5 \times w_1)\right)\right] - \left[C_6 \times w_1 \times \left((C_7 \times w_2) - (C_8 \times u_2)\right)\right]}$$

Where,

$$C_1 = \frac{V_{OC}}{2 \times R_{Batt} \times Q_{Batt_0}} \qquad C_2 = \frac{{V_{OC}}^2}{4 \times {R_{Batt}}^2 \times {Q_{Batt_0}}^2}$$

$$C_3 = \frac{\eta^k}{R_{Batt} \times {Q_{Batt_0}}^2} \times \left(\frac{\rho}{1+\rho}\right) \qquad C_4 = \frac{1}{R_{Batt} \times {Q_{Batt_0}}^2} \times \left(\frac{1+\rho}{\rho}\right)$$

$$C_5 = \frac{1}{R_{Batt} \times {Q_{Batt_0}}^2 \times R_t \times r_{final} \times \rho} \qquad C_6 = \frac{\eta^k}{R_{Batt} \times {Q_{Batt_0}}^2 \times R_t \times r_{final}}$$

$$C_7 = \frac{r_{final}}{R_{Batt} \times {Q_{Batt_0}}^2} \qquad C_8 = \frac{1}{R_{Batt} \times {Q_{Batt_0}}^2} \times \left(\frac{1}{1+\rho}\right)$$